Geosphere

Geomorphic response of submarine canyons to tectonic activity: Insights from the Cook Strait canyon system, New Zealand

--Manuscript Draft--

Manuscript Number:	GS1040R2
Full Title:	Geomorphic response of submarine canyons to tectonic activity: Insights from the Cook Strait canyon system, New Zealand
Short Title:	Control of active tectonics on submarine canyons
Article Type:	Research Paper
Keywords:	submarine canyons; active margin; tectonics; knickpoints; New Zealand
Corresponding Author:	Aaron Micallef University of Malta Msida, Msida MALTA
Corresponding Author Secondary Information:	
Corresponding Author's Institution:	University of Malta
Corresponding Author's Secondary Institution:	
First Author:	Aaron Micallef
First Author Secondary Information:	
Order of Authors:	Aaron Micallef
	Joshu J Mountjoy
	Philip M. Barnes
	Miquel Canals
	Galderic Lastras
Order of Authors Secondary Information:	
Abstract:	Active margins host more than half of submarine canyons worldwide. Understanding the coupling between active tectonics and canyon processes is required to improve modeling of canyon evolution and derive tectonic information from canyon morphology. In this paper we analyze high resolution geophysical data and imagery from Cook Strait canyon system (CS), offshore New Zealand, to characterize the influence of active tectonics on the morphology, processes and evolution of submarine canyons, and to deduce tectonic activity from canyon morphology. Canyon location and morphology bear the clearest evidence of tectonic activity, with major faults and structural ridges giving rise to sinuosity, steep and linear longitudinal profiles, cross-sectional asymmetry, and breaks in slope gradient, relief and slope-area plots. Faults are also associated with stronger and more frequent sedimentary flows, steep canyon walls that promote gully erosion, and seismicity that is considered the most likely trigger of failure of canyon walls. Tectonic activity gives rise to two types of knickpoints in CS. Gentle, rounded and diffusive knickpoints form due to short wavelength folds or fault break outs. The more widespread steep and angular knickpoints have migrated through canyon floor slope failures and localized quarrying/plucking. Migration is driven by base level lowering due to regional margin uplift and deepening of lower Cook Strait Canyon, and is likely faster in larger canyons because of higher sedimentary flow throughput. The knickpoints, non-adherence to Playfair's Law, linear longitudinal profiles and lack of canyon-wide, inverse power-law slope-area relationships indicate that the CS is in a transient state, adjusting to perturbations associated with tectonic displacements and changes in base level and sediment fluxes. We conclude by inferring unmapped faults and regions of more pronounced uplift, and proposing a generalized model for canyon geomorphic evolution in tectonically-active margins.

Cover Letter

Click here to download Cover Letter: Cover letter.doc

Manuscript submitted to Geosphere:

Geomorphic response of submarine canyons to tectonic activity: Insights from the Cook Strait canyon system, New Zealand.

Aaron Micallef [a,b]*, Joshu J. Mountjoy [c], Philip M. Barnes [c], Miquel Canals [b], Galderic Lastras [b]

[a] Department of Physics, Faculty of Science, University of Malta, Msida, MSD 2080, Malta.

[b] GRC Geociències Marines, Facultat de Geologia, Universitat de Barcelona, E-08028 Barcelona, Spain.

[c] National Institute of Water and Atmospheric Research, Private Bag 14901, Wellington, New Zealand.

*Corresponding author:

E-mail: aaron.micallef@um.edu.mt; Telephone: +356 23403613.

ABSTRACT

Active margins host more than half of submarine canyons worldwide. Understanding the coupling between active tectonics and canyon processes is required to improve modeling of canyon evolution and derive tectonic information from canyon morphology. In this paper we analyze high resolution geophysical data and imagery from Cook Strait canyon

system (CS), offshore New Zealand, to characterize the influence of active tectonics on the morphology, processes and evolution of submarine canyons, and to deduce tectonic activity from canyon morphology. Canyon location and morphology bear the clearest evidence of tectonic activity, with major faults and structural ridges giving rise to sinuosity, steep and linear longitudinal profiles, cross-sectional asymmetry, and breaks in slope gradient, relief and slope-area plots. Faults are also associated with stronger and more frequent sedimentary flows, steep canyon walls that promote gully erosion, and seismicity that is considered the most likely trigger of failure of canyon walls. Tectonic activity gives rise to two types of knickpoints in CS. Gentle, rounded and diffusive knickpoints form due to short wavelength folds or fault break outs. The more widespread steep and angular knickpoints have migrated through canyon floor slope failures and localized quarrying/plucking. Migration is driven by base level lowering due to regional margin uplift and deepening of lower Cook Strait Canyon, and is likely faster in larger canyons because of higher sedimentary flow throughput. The knickpoints, non-adherence to Playfair's Law, linear longitudinal profiles and lack of canyon-wide, inverse power-law slope-area relationships indicate that the CS is in a transient state, adjusting to perturbations associated with tectonic displacements and changes in base level and sediment fluxes. We conclude by inferring unmapped faults and regions of more pronounced uplift, and proposing a generalized model for canyon geomorphic evolution in tectonically-active margins.

Keywords: submarine canyons; active margin; tectonics; knickpoints; New Zealand

1. INTRODUCTION

Submarine canyons have long been recognized as principal sediment-transfer conduits that play an integral role in many aspects of continental margin development (Shepard, 1981; Normark and Carlson, 2003; Allen and Durrieu de Madron, 2009; Canals et al., 2013). The majority of published studies on canyon inception and development have been based on passive margin systems (e.g. Twichell and Roberts, 1982; Farre et al., 1983; Pratson et al., 1994; Pratson and Coakley, 1996; Pratson et al., 2009). However, active tectonic margins comprise a significant proportion of global continental margins and host more than half of submarine canyons worldwide (Harris and Whiteway, 2011). The morphology and evolution of canyons incising active margins are governed by climatic, sedimentary and oceanographic processes that are similar to those on passive margins, although tectonism tends to exert a predominant control at both local and regional scales. In particular, seafloor deformation, through folding, faulting, uplift or subsidence, has been shown to directly affect the location, alignment and geometry of many submarine canyons and channels worldwide; large-magnitude earthquakes, on the other hand, tend to influence facies distribution (e.g. Normark and Curray, 1968; Nagel et al., 1986; Lewis and Barnes, 1999; Laursen and Normark, 2002; Chiang and Yu, 2006; Le Dantec et al., 2010). Furthermore, canyons incising active margins tend to be shorter, steeper, and more dendritic and closely spaced than their counterparts in passive margins (Harris and Whiteway, 2011). Whilst excellent quality ultra-high resolution Autonomous Underwater Vehicle bathymetric data demonstrate detailed morphology of some canyon systems (e.g. Paull et al., 2011), most studies concerning canyons in active margins have

been based on coarse-resolution bathymetric data, which only provide useful information on macro-scale morphology. Detailed examination of relationships between active tectonics, seafloor processes and canyon development can only be made with continuous-coverage, high resolution bathymetric and seismic reflection data. It is therefore likely that the distinctive influence of active tectonics on submarine canyon morphology and processes has not been fully explored.

Tectonic geomorphology is a thriving field of subaerial geomorphology that examines the dynamic coupling between tectonics, climate and erosion (Crosby and Whipple, 2006; Bishop, 2007; Whipple, 2009; Brocklehurst, 2010). The focus of tectonic geomorphology has been the fluvial network which, by maintaining a direct connection to tectonic forcings, contains useful information on tectonic activity across a landscape (Wobus et al., 2006). Terrestrial river systems are known to respond to tectonics in several ways. Experimental results and field examples show how slope steepening due to uplift results in an increase in river sinuosity and convexity, as well as localized aggradation and degradation (Ouchi, 1985). Fault rupture to the land surface across a river bed can induce significant channel steps that propagate upstream. For example, the 1999 Chi-Chi earthquake produced surface offsets of 0.5 – 8 m that evolved upstream as a series of knickpoints of up to 18 m height over a period of 9 years (Yanites et al., 2010). Regionally high uplift rates affecting the entire channel reach can alter the equilibrium profile of a fluvial system and induce knickpoint propagation up a riverbed until the system re-attains some equilibrium state (Snyder et al., 2000). Reduction in post-glacial sediment supply can also drive knickpoint development and migration in some river

systems (e.g. Berryman et al., 2010). Another response is the dramatic and long lasting increase in sediment load due to earthquake-induced slope instability (Dadson et al., 2004). Many studies have dealt with quantitative analyses of digital elevation models, particularly focusing on channel morphology, to obtain information on the character, pattern and rates of tectonic deformation, and to develop long-term landscape evolution models (e.g. Howard, 1994; Burbank et al., 1996; Demoulin, 1998; Whipple and Tucker, 1999; Snyder et al., 2000; Kirby and Whipple, 2001; Snyder et al., 2003; Whittaker et al., 2008; Sougnez and Vanacker, 2011). Our ability to derive similar information from submarine canyon topography is severely limited by several factors. These include the paucity of data available to develop and calibrate process-based laws, the difficulties in obtaining in situ measurements of sediment flows, and the inapplicability of surface exposure dating techniques underwater (Huyghe et al., 2004; Mitchell, 2006). Knowledge of the effects of active tectonics on submarine canyon development is thus still insufficient to enable quantitative studies of canyon evolution. Considering that most data available from submarine canyons are morphological, a better understanding of the coupling between active tectonics and submarine canyon morphology and processes is required.

In subaerial geomorphology, the stream power erosion model has have been developed to relate the fluvial erosive process to larger-scale landscape form. In many settings, local channel slope (S) and contributing drainage area (A) have been shown to be related by an inverse power law scaling (Flint, 1974; Howard, 1994; Whipple and Tucker, 2002):

$$S = k A^{-\theta} \quad (1)$$

where k is the steepness index and θ is the concavity index. Inverse power law scaling in bedrock-eroding rivers has been interpreted to arise where there is a steady state between tectonic uplift and erosion. Thus, segments of individual slope-area profiles characterized by different values of steepness and concavity indices are often used to extract tectonic information from the landscape (Wobus et al., 2006). Channel steepness, in particular, has been predicted to correlate with rock uplift rates (Howard, 1994). These relationships are based on several assumptions, and their applicability are limited by many complexities, such as non-linearities in incision processes, adjustments in the channel, bed morphology or sediment size, and changes in climate or tectonic state (Whipple and Tucker, 1999; Snyder et al., 2000; Whipple and Tucker, 2002; Snyder et al., 2003). On the continental margins of the Atlantic USA and Taiwan, slope-area relationships similar to those reported for subaerial rivers have been shown to be common for submarine canyons (Mitchell, 2004, 2005; Ramsey et al., 2006; Brothers et al., 2013). The relationships for submarine canyons have been explained by a model where the frequency of flows experienced by the canyon increases downstream and with increasing contributing area, representing the upstream area of canyon walls with potentially unstable sediment capable of sourcing erosive sedimentary flows. In this model, erosion in the continental slope progresses towards a form of spatial equilibrium so that channels have concave-upwards long-profiles, with the downstream effect of increasing flow frequency being balanced by decreasing gradient. It is very difficult to corroborate this model with field data. The origin of the slope-area relationships is still unclear because

139 erosion by rivers and gravity flows differs in many aspects, particularly in terms of
140 density contrast, thickness, and flow transformation. Submarine canyons are
141 characterized by increasingly resistant lithology with depth, flank slope failures, spatial
142 and temporal changes in erosion mechanisms, and varied sediment input. The
143 downstream change in dynamical behavior of submarine gravity flows is quite different
144 from that of rivers because of the increase or loss of flow power with suspension or
145 deposition of particle load (Gerber et al., 2009). It has also been suggested that drainage
146 basin area in submarine canyons is not related to flow discharge as in terrestrial systems,
147 but results from the aggregation of random walks (Straub et al., 2007). The details of
148 submarine flow processes and their interaction with seafloor morphology and tectonic
149 processes are therefore still too vague to justify using morphological parameters to
150 extract tectonic information.
151
152 The purpose of this study is to carry out morphological and morphometric analyses of
153 high resolution bathymetric and seismic reflection data from the Cook Strait canyon
154 system (CS), which incises the Hikurangi Margin off New Zealand's North Island, to: (i)
155 understand how tectonic activity influences submarine canyon morphology, processes
156 and evolution in an active margin, (ii) deduce current or past tectonic activity across the
157 Hikurangi Margin, and (iii) formulate a generalized model of canyon development in
158 response to tectonic forcing based on morphometric parameters. Addressing these
159 research objectives is important for developing a framework for reconstructing and
160 predicting canyon dynamics in active margins, which has direct implications also for
161 canyon oceanography and biology, as well as deriving tectonic information from canyon

morphology, which can improve offshore neo-tectonic analyses and hazard assessment. Cook Strait is an excellent site to investigate the signature of tectonism in submarine canyons - it comprises an active subduction-to-strike slip tectonic margin that is traversed by a series of active thrust and strike-slip faults, incised by New Zealand's largest submarine canyon system, covered by high resolution seafloor data (Mountjoy et al., 2009; Lamarche et al., 2011) and there is excellent quality seismic reflection data available for subsurface imaging of stratigraphy and tectonic structure. The tectonic strain rates from GPS data, and the ground shaking potential from earthquake sources from paleoseismic and seismological studies, are very well known in this area, providing an excellent framework to assess the response of canyons to tectonic forcing.

2. REGIONAL SETTING

2.1 General setting and geomorphology

Cook Strait is the seaway between the North and South Islands of New Zealand and links the Tasman Sea with the Pacific Ocean (Figure 1). The strait narrows to 22 km width at the central neck, and widens towards the north and south. The majority of the seabed is at water depths of less than 150 m; the exceptions are the Narrows Basin, where depths exceed 300 m, and to the south-east of the Cook Strait. The seaway is subjected to strong tides, sustaining flows of 1.5 - 2 m s^{-1} over large areas, which are known to mobilize sediment up to cobble size (Carter et al., 1991; Stevens et al., 2012; Mountjoy et al., 2013). Active faults underlie the continental shelf (Barnes and Audru, 1999a; Pondard

and Barnes, 2010), although the morphology of the shelf is strongly affected by tidal current scour and deposition (Lamarche et al., 2012a; Lamarche et al., 2012b). Beyond the continental shelf, active tectonic deformation is a primary driver of large scale seafloor geomorphology, and is known to have a significant influence on the canyon system (Mountjoy et al., 2009). This region of the Hikurangi Margin is referred to as the Cook Strait sector (Figure 1).

2.2 Tectonic setting, active deformation and earthquake sources

The CS is located on the southern Hikurangi Margin subduction system (Mountjoy et al., 2009) (Figure 1). Subduction of the Pacific Plate underneath the Australian Plate is occurring at a rate of ~38 mm yr^{-1} at 050° oblique to the plate margin (Beavan et al., 2002). Slip partitioning results in an orthogonal convergence at a rate diminishing from ~20 mm yr^{-1} north of Cook Strait, to ~ 6 mm yr^{-1} south of the strait (Wallace et al., 2004). The convergence results in numerous active upper-plate thrust and strike-slip faults occurring throughout the region (Figure 2a; Barnes and Audru, 1999a, b; Pondard and Barnes, 2010; Plaza-Faverola et al., 2012; Wallace et al., 2012; Henrys et al., 2013). Thrust faulting beneath the continental slope is expressed as margin-parallel ridges that reflect anticline development. Palliser and Opouawe banks are examples of folding and bathymetric uplift in the hanging wall of northwest-dipping thrust faults (Figures 1, 2a).

Active faults have been incorporated into the New Zealand National Seismic Hazard Model as generalized earthquake sources derived from quantification of active fault

parameters across New Zealand (Stirling et al., 2012; Litchfield et al., 2013). The CS is expected to experience ground shaking levels of 0.4 - 0.6 g over the 1000-year return period (Figure 3a; Stirling et al., 2012). Mean vertical slip rates for the faults crossing the lower CS vary from 1 - 4 mm yr^{-1} based on structural restorations and slip deficits (Barnes and Mercier de Lepinay, 1997; Wallace et al., 2012). Strike-slip faults crossing the upper canyon have horizontal rates of 4 - 12 mm yr^{-1}, with very little overall vertical slip (Stirling et al., 2012). Single event displacements expected during coseismic rupture of each of the faults are shown in Figure 3a.

Two large earthquakes have occurred in the Cook Strait in historical, pre-instrumental times - the 1848 M7.5 Marlborough event and the 1855 M8.2 Wairarapa Earthquake (Grapes and Downes, 1997; Grapes et al., 1998). Most recently, on the 21 July and 16 August 2013 two earthquakes (M6.5 and M6.6, respectively) occurred on offshore faults beneath the continental shelf of south-western Cook Strait. The shaking from these latter events was widely felt but no surface rupture or geomorphic response was observed in post-event offshore surveys (Mountjoy, 2013). The potential for mega-thrust earthquakes on the Hikurangi Margin is poorly constrained, partly as no large historical events have occurred, and partly due to poor paleoseismologic evidence (e.g. Clark et al., 2011). Dislocation modeling for a hypothetical M9 subduction earthquake rupturing the entire length of the Hikurangi Margin, and accounting for approximately 1000 years of strain accumulation, results in up to 2 m vertical motion across the lower part of CS and subsidence of up to 2 m around the upper-most canyon (Fraser et al., 2014) (Figure 3b).

2.3 Submarine canyons

The CS comprises five major canyons, the flanks of which are characterized by numerous gully systems and landslide scars (Figure 1). Cook Strait Canyon is recognized as the major through-going feature extending from the shelf to the Hikurangi Channel at the toe of the margin (Mountjoy et al., 2009). In this paper we distinguish between the upper and lower reaches of the Cook Strait Canyon because they have distinctly different morphology and morphometrics. Nicholson, Wairarapa, and Palliser Canyons, and a relatively small canyon referred to informally here as Boo Boo Canyon, are tributaries that feed into Cook Strait Canyon. Campbell and Opouawe Canyons are single branch canyons that also connect to the Hikurangi Channel, but not to the Cook Strait Canyon (Figure 1). Canyon rims occur as shallow as 50 m on the continental shelf, and exit to the Hikurangi Channel at depths greater than 2500 m.

Nicholson, Wairarapa, and the middle to upper reaches of Cook Strait Canyon are incised in Late Cenozoic sedimentary sequences of indurated and gently dipping mudstone, siltstone or sandstone (Mountjoy et al., 2009). The northern walls of Nicholson and Wairarapa Canyons may expose Torlesse Greywacke Mesozoic basement, consisting of well-indurated and slightly metamorphosed mudstones and silty sandstones. Palliser, Opouawe, Campbell, Boo Boo and the deeper part of Cook Strait Canyons are incised in Neogene slope and uplifted basin-floor turbidite sequences (Uruski, 2010).

253 The canyons can be divided in two groups. The upper canyons (Nicholson, Wairarapa
254 and upper Cook Strait Canyons) incise the continental shelf, whereas the lower canyons
255 (Palliser, Opouawe, Campbell, Boo Boo and lower Cook Strait Canyons) incise the
256 continental slope. The morphological characteristics of each canyon are presented in
257 Table 1.
258
259 ## 3. DATA SETS
260
261 ### 3.1 Multibeam echosounder data
262
263 This study is mainly based on 8400 km^2 of multibeam echosounder data collected
264 between 2002 and 2005 using a hull-mounted Simrad EM300 multibeam system
265 operating at a 30 kHz frequency, and a POS/MV system with differential Global
266 Positioning System, on board the RV *Tangaroa*. The navigational accuracy and vertical
267 accuracy of the multibeam echosounder data in 1000 m water depth are ±5 m and ±2 m,
268 respectively. Bathymetry and backscatter data grids of 10 m × 10 m bin size were derived
269 from the multibeam echosounder data. The bathymetry data were processed with C&C
270 Technologies HydroMap software by accounting for sound velocity variations and tides,
271 and by implementing basic quality control. The backscatter data were processed with
272 SonarScope software developed by IFREMER (Augustin and Lurton, 2005). Processing
273 included signal calibration and compensation, speckle noise filtering, texture analysis and
274 image segmentation (Lamarche et al., 2011).
275

3.2 Multichannel seismic reflection profiles

Wide-angle, deep penetration multichannel seismic reflection (MCS) data were collected from the Cook Strait sector of the Hikurangi Margin in 2009-2010 (Ministry of Economic Development, 2010). Twenty six 2D seismic profiles were acquired during the Pegasus survey and processed to pre-stack time migration by GeoTrace (2010). These include five dip lines across the margin of the CS (PEG10-09 to -19), with an average line spacing of ~15 km, and two strike lines (PEG10-02 and -04).

3.3 DTIS

During research cruise TAN1103 carried out on board the RV *Tangaroa* in 2011, we acquired high definition video and still imagery of the seabed along four transects in Nicholson, Wairarapa and Cook Strait Canyons using NIWA's Deep Tow Imaging System (DTIS). Real-time data processing and recording were carried out using the Ocean Floor Observation Protocol (OFOP) software.

4. METHODOLOGY

Standard morphometric attributes (slope gradient, slope aspect, profile and plan curvature) were extracted from the bathymetric data set using the Geographic Information System ESRI ArcGIS. Submarine gullies and canyon thalwegs were automatically mapped using standard GIS hydrology tools for terrestrial drainage

299 network extraction, which included the computation of “flow direction” and “flow
300 accumulation” routines across the study area after sinks in the grid were infilled (Tubau
301 et al., 2013). The resulting maps were validated via a thorough visual inspection. Canyon
302 longitudinal profiles were extracted along the automatically mapped canyon thalwegs.
303 Morphological steps along the canyon floor were identified from slope gradient
304 longitudinal profiles using a moving average that estimated the general trend of the slope
305 gradient and eliminated peaks due to fine-scale roughness. The boundaries of submarine
306 landslide scars were delineated from a geomorphometric map and an automated
307 topographic classification (using the standard deviation of slope gradient) generated from
308 the bathymetry data set using techniques described in Micallef et al. (2007). The
309 boundaries of submarine canyons were delineated semi-automatically using
310 morphometric attribute maps (slope gradient, slope aspect, profile curvature), the flow
311 accumulation map, and the geomorphometric map. These maps clearly identify the
312 pronounced and subtle changes in morphology along the canyon borders. The resolution
313 of the maps is equivalent to the resolution of the bathymetric data, rather than the scale at
314 which the landscape is being interpreted by the user (Micallef et al., 2007). Canyon relief
315 was calculated by interpolating the bathymetry grid across the boundaries of submarine
316 canyons and subtracting from the original bathymetry.
317
318 Thalweg slope gradient and upslope canyon area were extracted at 20 m isobath intervals
319 along the floor of each canyon to generate slope-area plots (Brothers et al., 2013). Power
320 law trend lines were fitted to the plots, from which the exponent (concavity index) and
321 co-efficient (steepness index) were derived from the power law equation. The plots

322 comprised different segments of data points, which can be distinguished in terms of the
323 trend followed by the data and the values of concavity and steepness indices. The
324 division of the plots into segments was guided by a moving average calculated for all the
325 data points in each plot. The theoretical and methodological background of slope-area
326 plots is provided by Wobus et al. (2006).
327
328 Base level in the submarine environment has been defined as the deepest point in the
329 basin that can be reached by sedimentary gravity flows (Carter, 1988; Amblas et al.,
330 2011; Georgiopoulou and Cartwright, 2013). For this study, the regional base level of the
331 study area is interpreted to lie at 2700 m depth and located in the Hikurangi Trough
332 (CANZ, 2008).
333
334 Tectonic structures beneath the lower reaches of the CS were mapped in this study using
335 the high-fold Pegasus seismic survey profiles (Geotrace, 2010), archived single-channel
336 and low-fold multichannel seismic profiles (Barnes et al., 1998; Mountjoy et al., 2009),
337 and the multibeam bathymetric data.
338
339 ## 5. RESULTS
340
341 ### 5.1 Reinterpretation of active faulting and folding across the lower CS
342
343 Multibeam bathymetric data show a series of linear scarps extending along the steep
344 forelimb (downslope-facing) slopes of anticlinal ridges (e.g. Opouawe-Uruti Fault and

345 Pahaua Fault; Figure 1). These scarps were interpreted by Mountjoy et al. (2009) as fault
346 tip lines associated with the major thrust faults controlling ridge propagation. Until now it
347 was unclear whether or not faults continued across lower Cook Strait Canyon. In the new
348 Pegasus MCS data the observed linear scarps cannot be associated with fault tip
349 breakouts, and most of the major thrusts have blind tips beneath the forelimb of the
350 anticlinal ridges. An example is shown in Figure 4, where a blind thrust tip-related to a
351 major splay fault crossing the lower Cook Strait Canyon is developing a well formed
352 anticline with long term uplift rates in the order of 1.1 ± 0.4 mm yr^{-1} (Barnes et al., 1998).
353 In Opouawe Canyon, splay faults do outcrop at the seafloor (Figure 2b), and in map view
354 extend along the seaward margin of the canyon floor.
355
356 **5.2 Canyon morphology**
357
358 The large-scale morphology of the CS as a whole has been described by Mountjoy et al.
359 (2009). The canyon network pattern is dendritic with three main canyons (Cook Strait,
360 Opouawe and Campbell Canyons) and four tributary canyons (Nicholson, Wairarapa,
361 Palliser, Boo Boo Canyons), most of them sinuous in planform. Where the canyon system
362 intersects a thrust fault (e.g. Wharekauhau fault), strike-slip fault (e.g. Boo Boo, Needles
363 faults) or a tectonic ridge (e.g. Palliser and Opouawe Banks), there is a change in
364 direction or offset of the canyon axis (e.g. Wairarapa, Cook Strait Canyons) (Figure 1).
365 Palliser, Opouawe and Boo Boo Canyons are also parallel to thrust faults, including the
366 Opouawe-Uruti and Pahaua faults (Barnes et al., 2010). Where the canyon intersects a
367 strike-slip fault (e.g. Needles, Wairarapa faults), the canyon is wider downslope (e.g.

368 Nicholson, Cook Strait Canyons) (Figure 1). The floors of the upper canyons, excluding
369 the upper sections of Cook Strait and Nicholson Canyons, are characterized by a low
370 backscatter (Figure 5a). In comparison, the floors of the lower canyons are associated
371 with higher backscatter.
372
373 In cross-section, the canyons are generally V-shaped, with the floors widths reaching up
374 to 2.5 km. The canyon walls comprise the steepest terrain across this part of the
375 Hikurangi margin, locally reaching slope gradients of 30°. Some of the canyon walls,
376 such as those of Wairarapa, Palliser, Opouawe and Boo Boo Canyons, are parallel to
377 faults (Figure 1). The canyon walls are also asymmetric, with opposing walls of
378 individual canyons showing a difference of up to 10° in slope gradient. The canyon walls
379 have been eroded by either linear to dendritic gullies (Micallef and Mountjoy, 2011), or
380 submarine landslides (Micallef et al., 2012) (Figure 5c-d). The highest gully densities are
381 observed in the lower canyons (Table 1). There are 141 landslide scars on the walls of the
382 CS; these have been interpreted as resulting from deep-seated, translational landslides
383 occurring in Late Cenozoic to Pleistocene sequences (Mountjoy et al., 2009; Micallef et
384 al., 2012). The landslide scars are located across the entire depth range covered by the
385 canyons, although 65% of the scars (by area) occur in the shallow canyons (Figure 5c).
386 The landslides scars are predominantly small, with median area and volume of 0.82 km^2
387 and 0.013 km^3, respectively.
388
389 Estimated relief along the canyon thalwegs ranges between 330 m and 1200 m (Figure
390 5b); the highest values are recorded in the lower canyons (Table 1). All canyons show a

general increase in relief with distance down canyon. Abrupt changes in relief across canyons coincide with faults (Figure 5b).

5.3 Longitudinal profiles

The longitudinal profiles of the CS vary from convex (upper Cook Strait Canyon), to linear (lower Cook Strait, Boo Boo, Opouawe, Palliser and Wairarapa Canyons) to slightly concave (Nicholson and Campbell Canyons) (Figure 6). Breaks and concave changes in the longitudinal profile predominantly coincide with known faults (Figure 7). The steepest mean thalweg slope gradients are observed in the lower canyons (Table 1). We also note that Palliser and Boo Boo Canyons appear to be hanging above the lower Cook Strait Canyon.

5.4 Steps and depressions

The longitudinal profiles of the canyons are interrupted by twenty eights steps and eight depressions, 92% of which occur in the lower canyons (Figures 7; 8). The steps consist of individual convex to concave changes in slope that are generally associated with high backscatter. The depressions, all of which are located downstream of the mouth of lower Cook Strait Canyon, are smaller, occur in groups, and have upslope asymmetrical wave-like shapes in profile.

413 The heights and slope gradients of the steps vary between 20 m and 233 m, and 2.3° and
414 34.8°, respectively. All the steps correspond to the upper limits of crescent-shaped scars
415 on the canyon floor, only a few of which extend across the entire canyon width. The
416 higher and steeper the steps are, the more likely the scar extends across the entire canyon
417 floor. Downslope of some of the steps, the canyon walls have abundant landslide scars
418 (Figure 7d; Micallef et al., 2012). At least 4 steps (1, 17, 18, 28) have rounded lips, and
419 are associated with low backscatter and with either faults or with propagating folds
420 related to blind faults. The remaining steps have more angular lips, and the canyon floor
421 downslope of the steps is associated with high backscatter. Half of the steps have a ridge
422 at their base. DTIS-31 imagery of the seafloor downslope of step 4, located in the lower
423 Cook Strait Canyon, shows the occurrence of bedrock containing rock mass defects
424 exposed at the seafloor, large tabular and sub-angular blocks of mudstone, and angular
425 fragments of mudstone scattered across the canyon floor (Figures 7h; 8).
426
427 We measured the distance along the seabed of steps from either the regional base level or
428 the floor of the canyon in which a tributary canyon hosting the step drains. Figure 9 is a
429 plot showing how some of these steps from Cook Strait, Palliser and Boo Boo Canyons
430 can be classified into three groups (steps 7 and 12; steps 11 and 14; steps 3, 10 and 13)
431 according to their distances from the floor of lower Cook Strait Canyon. We also plotted
432 the total canyon area against the distance of steps in the lower canyons from their local
433 base levels; the resulting plot shows a good power law relationship between these two
434 variables (Figure 10).
435

5.5 Slope-area analyses

The thalweg slope-area plots for each submarine canyon are shown in Figure 11. The majority of the boundaries of the plot segments coincide with either a fault and/or a step (Figure 11). The power regression models fitted to the segments identified for each plot are predominantly characterized by low coefficients of determination (R^2). The lowest R^2 and the highest concavity index values coincide with segments of the canyons located in between faults and/or steps. The highest R^2 values for the inverse power law regression models occur in Nicholson and Wairarapa Canyons, and the upslope segment of Boo Boo Canyon, all of which are located upslope of faults or steps. Segments with the highest values of mean slope gradient have been mapped in Figure 12. These correspond to the upper and lower reaches of Campbell, Palliser, and Boo Boo Canyons, and the lower reaches of Opouawe Canyon. Where not coinciding with the canyon heads, segments with the highest mean slope gradients are associated with canyon areas located upslope of either faults or steps.

6. DISCUSSION

6.1 CONTROL OF TECTONICS ON CANYON MORPHOLOGY, PROCESSES AND EVOLUTION

6.1.1 Control of active tectonics on canyon morphology

The clearest influence of active tectonic deformation on canyons is in terms of location and planform shape. Alignment and proximity of Wairarapa, Palliser, Opouawe and Boo Boo Canyons with faults indicates that canyon erosion is likely to have taken place along traces of major faults or has been constrained by structurally-generated tectonic ridges. This would have taken place by steepening of the seabed associated with tectonic growth, diversion/focusing of gravity flows by topographic steps or lips, or dense fracturing of the bedrock by faults. At a first order, the dendritic and sinuous pattern of the CS is thus predominantly a result of the numerous thrust and strike-slip faults that intersect the canyon system at various angles (5° - 90°) across the continental shelf and slope. The new MCS data confirm that the tectonic ridges that are responsible for the sinuosity of the lower Cook Strait Canyon are active anticlines (Figure 4). The upper Cook Strait, Nicholson and Opouawe Canyons also show that canyon widening has occurred downslope of strike-slip faults intersecting the canyon axes. This is a result of the lateral shifting of the focus of erosion due to the displacement of the canyon by fault movement.

481 The occurrence of tectonic ridges is also partly responsible for the asymmetry observed
482 in walls of the lower canyons because the forelimbs of the tectonic ridges in Cook Strait
483 are up to two times steeper than their backlimbs (upslope-facing) (Mountjoy et al., 2009).
484 The longitudinal profiles of the CS are steep (mean thalweg slope gradient of up to 5.74°;
485 Table 1) and predominantly linear. Both of these morphological characteristics are a
486 result of active tectonic deformation steepening the continental slope and being more
487 effective than incision by sedimentary flows (Huyghe et al., 2004; Covault et al., 2011).
488
489 The morphological patterns identified so far are similar to those documented in other
490 submarine canyons in tectonically active margins, e.g. La Jolla Canyon (Le Dantec et al.,
491 2010), Monterey Canyon (Greene et al., 2002), San Antonio Canyon (Laursen and
492 Normark, 2002), Kushiro Canyon (Noda et al., 2008), Kaoping Canyon (Chiang and Yu,
493 2006) and submarine channels in the Nankai Trough (Alves et al., in press). These
494 patterns, together with the breaks/changes observed in canyon longitudinal slope profiles
495 and mean slope gradient, relief and slope-area plots where the canyons intersect faults
496 (Figures 5b; 7; 11, 12), indicate that tectonic activity leaves a clear topographic signature
497 on the canyon morphology. These results are also similar to what has been reported for
498 subaerial fluvial systems (e.g.Whipple, 2004; Wobus et al., 2006).
499
500
501
502
503

6.1.2 Control of active tectonics on canyon processes and evolution

(a) Sedimentary flows

The high backscatter observed in the Opouawe Canyon is a response to the occurrence of gravel (Geoffroy Lamarche, pers. comm), and in lower Cook Strait Canyon is due to dense sand (Philip Barnes, pers. comm.). Assuming that, for the entire CS, a high backscatter signal is indicative of coarser sediment or bedrock exposures (Mitchell, 1993a; Lamarche et al., 2011), we infer that the higher backscatter in the lower canyons, in comparison to the upper canyons, is indicative of a lack of fine-grained sediment of a certain thickness (Mitchell, 1993b). This implies that the sediment has been eroded by currents with velocities higher than the threshold of motion of fine-grained sediment. We suggest that this is a result of stronger, more frequent or more recent sedimentary flows (and the associated reduction in sediment deposition and increase in bedrock exposure) where thrust faults are located. The origin of these flows is likely earthquake-triggered mass wasting and knickpoint migration (see 6.1.2(c)). The high backscatter and inferred high canyon flow in the upper Cook Strait and Nicholson Canyons, on the other hand, is associated with remobilization of sediment deposited by tidal currents and earthquake triggering of mass wasting events in the upper canyons (Mountjoy et al., 2013).

(b) Submarine gullies and landslides

Submarine gully erosion in the Cook Strait sector occurs above a threshold slope gradient of 5.5° (Micallef and Mountjoy, 2011). Since the more intense gully erosion is observed on the walls of the lower CS, we suggest that active tectonics play a direct role in promoting submarine gully erosion by generating steep terrain. Submarine gullies, in turn, contribute to canyon evolution by establishing the template along which submarine canyons grow (as in Tubau et al., 2013; Vachtman et al., 2013). Submarine landslides, on the other hand, are mostly located in the upper canyons, where vertical tectonic deformation is the least pronounced as faults are predominantly strike-slip. This confirms that landslide preconditioning is mostly related to canyon incision and wall undercutting. In addition, Cenozoic sedimentary basins within which the upper canyons have formed are less tectonically deformed than units underlying the continental slope, resulting in stratigraphic geometries that are more prone to large bedding-parallel slope failure. Earthquake-generated ground motion is likely to be the primary slope-failure triggering mechanism for most landslides, however, and will act as a secondary preconditioning factor via slope deformation or generation of excess pore pressures in high permeability horizons (Sultan et al., 2004; Mountjoy et al., 2009; Mountjoy et al., 2013). Irrespective of their causes, submarine landslides have an important influence in canyon evolution by eroding walls, extending canyons laterally, and introducing material into the canyon floor (Micallef et al., 2012).

(c) Knickpoint formation and evolution

In the CS, the morphology and location of some steps, such as those in Nicholson (step 1), upper Opouawe (steps 17 and 18) and lower Opouawe (step 28) Canyons, reflect deformation of the canyon floor, either as short wavelength folds or fault break outs (e.g. Wharekauhau fault (Mountjoy et al., 2009)) (Figure 8). This explains the generally low slope gradients measured at these steps (Table 2). We suggest, however, that the majority of the steps across the CS have predominantly formed by slope failures on the canyon floor and localized quarrying and plucking, both driven by sedimentary flows. Our inference is based on morphological evidence - the crescent-shaped depressions on the canyon floor, which are likely the scars of rotational slope failures (e.g. Paull et al., 2011), and the ridges at their base and the sub-angular blocks observed on the DTIS imagery, which are evidence of slope failure and quarrying/plucking processes (Figure 7). Steps associated with slope failures and erosion have higher slope gradients than fold/fault-controlled steps, which is likely a result of landslides revealing more cohesive material whereas only shallow buried sediments are currently being eroded at folds/faults.

In view of the above, we interpret the steps as knickpoints, which in fluvial systems are defined as steep gradient sections between low gradient sections along a course (Howard, 1994). Submarine knickpoints have been widely reported in active tectonic margins (e.g. Kukowski et al., 2001; Orpin, 2004; Adeogba et al., 2005). In submarine canyon-channel systems, knickpoints are proposed to initiate either where tectonic motion has deformed

572 the seafloor (Soh and Tokuyama, 2002; Mitchell, 2006; Heiniö and Davies, 2007), or
573 where channel levées have been breached (Pirmez et al., 2000; Estrada et al., 2005).
574
575 In the CS, we differentiate between knickpoints associated to faults and folds, and
576 knickpoints formed by canyon floor slope failures and erosion. We also infer differences
577 in the way in which these two types of knickpoints have evolved. Knickpoints associated
578 to folds and faults diffuse (Figure 13), developing into smoother, gentler breaks of slope
579 through upstream erosion and downstream deposition by channelized sedimentary flows
580 until an equilibrium profile is restored (e.g. step 1 in Nicholson Canyon). This is similar
581 to the mechanisms of gradient adjustments reported in submarine channels (Kneller,
582 1995; Pirmez et al., 2000; Georgiopoulou and Cartwright, 2013) and it would explain the
583 lower backscatter observed along the canyon floor where such knickpoints are located. It
584 is compatible with knickpoint evolution in terrestrial alluvial fans (e.g. Paola, 2000), but
585 differs from examples of fault-induced knickpoint migration in river systems undergoing
586 detachment-limited erosion (e.g. Yanites et al., 2010).
587
588 Knickpoints formed by canyon floor slope failures and erosion, on the other hand, are
589 located upslope of both additional slope instabilities along the adjacent canyon walls
590 (Figure 7d) as well as canyon floors with high backscatter (Figure 5a), both of which we
591 interpret as suggesting upslope knickpoint migration. We propose that knickpoint
592 migration is driven by base level lowering (Figure 13). For the entire CS, the regional
593 base level is the Hikurangi Trough, which is lowered due to regional uplift of the margin
594 (Figure 3b). Given that the maximum coseismic uplift of the lower canyon system

595 associated with subduction earthquakes may be ~2 m (Figure 3b), it is likely that a major
596 period of knickpoint migration is initiated after several, rather than one, uplift events. The
597 upper reaches of the CS may have competing vertical tectonic processes from upper plate
598 fault rupture contrasting with inter-seismic and co-seismic subduction thrust deformation,
599 which led to ephemeral canyon longitudinal profile changes. Figure 3b, for example,
600 shows that Nicholson Canyon is expected to subside by up to 2 m during hypothetical
601 giant subduction earthquakes, whilst fault rupture during the M8 1855 Wairarapa
602 earthquake produced substantial coseismic uplift at Cape Turakirae (McSaveney et al.,
603 2006) and presumably uplift of the upper reaches of the CS. For Palliser and Boo Boo
604 Canyons, the base level is the lower Cook Strait Canyon floor, which is lowered by
605 canyon floor erosion. The latter is likely to have been affected by regional base level
606 lowering, but also by changing sediment fluxes associated with varying climates and sea
607 levels. During sea level lowstands associated with glacial periods, coarse clastic
608 sediments were fed directly into the heads of the upper CS canyons by terrestrial rivers
609 and longshore drift. This is likely to have led to entrenchment of the upper CS canyons
610 and transient aggradation of the Cook Strait Canyon (e.g. Mountain et al., 1996). Sea
611 level rise accompanying the transition into interglacial periods disconnected the upper CS
612 canyon heads from a direct sediment supply. Such a reduction in post-glacial sediment
613 supply is thought to have resulted in the erosion of older, lowstand canyon system and
614 initiated localized knickpoint migration (Mountjoy et al., 2009). We propose that the
615 knickpoint created by base level lowering migrates up canyon as an entrenchment
616 knickpoint that retrogressively down-cuts and erodes the lower CS. This erosion takes
617 place through slope failure and/or quarrying/plucking processes driven by sedimentary

618 flows (e.g. Pirmez et al., 2000; Mitchell, 2006; Toniolo and Cantelli, 2007; Amblas et al.,
619 2011; Turmel et al., 2011). Our inference is reinforced by the fact that the knickpoint lips
620 are angular, which is indicative of advective migration (Mitchell, 2006), as well as the
621 spatial association between knickpoints in Palliser, Boo Boo and upper Cook Strait
622 Canyons, which are shown to be located at a similar distance from their base level
623 (Figure 9). The latter is similar to what has been observed in subaerial fluvial systems,
624 where knickpoints recording transient conditions lie at a near constant elevation from the
625 base level (e.g. Niemann et al., 2001). The wall slope failures located downslope of the
626 knickpoints are likely to have been triggered by undermining and loss of support (Sultan
627 et al., 2007; Micallef et al., 2012). Knickpoints formed by canyon floor slope failures and
628 erosion are therefore evidence of a renewed phase of incision in the lower reaches of the
629 CS.
630
631 We do not exclude that, in the CS, knickpoints associated to faults also migrate upslope,
632 as documented by Mitchell (2006), or that knickpoints associated to slope failure also
633 diffuse. In our study area we do not have information on how the morphology of a
634 knickpoint changes as it translates upstream through the canyon system. However, it is
635 possible that a knickpoint degrades and reforms as it encounters regions of higher or
636 lower erodibility, as documented in submarine channels (Pirmez et al., 2000) and
637 subaerial fluvial systems (Crosby and Whipple, 2006).
638
639 In subaerial fluvial geomorphology, the stream power erosion model provides the most
640 popular quantitative tool to describe knickpoint retreat (Howard and Kerby, 1983; Bishop

et al., 2005; Crosby and Whipple, 2006). According to this model, knickpoint migration rate is a function of drainage area and local slope. The stream erosion model seems to be relevant to explain knickpoint evolution in the CS as well. Figure 10 shows a good positive relationship between the area of lower canyons and the distance of knickpoints from their local base level, the latter being indicative of the rate at which knickpoint migrate upslope. An incisional pulse triggered by a change in base level is thus likely to be best transmitted in the main Cook Strait Canyon and to be slower in its tributaries and the other canyons. The fact that knickpoints migrate fastest in the largest canyons is likely a result of a higher and more erosive volume of sedimentary flows. The inference that the erosive capacity of sedimentary flow increases with canyon area is also supported by numerical models (Pratson and Coakley, 1996; Pratson et al., 2000). Based on these considerations, the rate of knickpoint migration should also decrease with time because, as it moves upslope, the canyon drainage area is bound to decrease.

Knickpoint formation and evolution may be attributable to factors other than folds and faults, changes in base level, or changing sediment fluxes. A factor that cannot be completely ruled out is variation in lithological resistance (Miller, 1991; Mitchell, 2004; Phillips et al., 2010). We are unable to constrain the stratigraphy of the floor of the entire CS, and it is plausible that where stratigraphy is truncated by erosion, resistant beds along the floors may create canyon steps (e.g. ‘stratigraphy truncated by erosion’ in Figure 4b). On the other hand, it is unlikely that we would observe the morphologies and morphometric patterns described in section 5.4 if lithological resistance were the primary control of knickpoint formation and evolution. Thus we propose that the role of changing

lithological resistance in knickpoint formation and evolution is secondary and localized, although sediment/rock properties may help explain difference in knickpoint morphology.

(d) Cyclic steps

Spatially-periodic depressions occur downslope of the mouth of the lower Cook Strait Canyon, where sedimentary flows evolve from confined to unconfined conditions. We interpret these depressions as cyclic steps, which are manifestations of a fundamental morphodynamic instability of Froude-supercritical flow over an erodible bed (Parker and Izumi, 2000). Cyclic steps are long-wave erosional/depositional bedforms that are bounded by a hydraulic jump and that migrate upstream as a coherent, quasi-permanent train of permanent form (Fildani et al., 2006; Kostic, 2011). The upslope asymmetrical shape of cyclic steps in CS is indicative of a low energy setting because of a decrease in vertical thickness and velocity, and a resulting drop in the Froude number, due to spreading of the flow at the canyon mouth (Cartigny et al., 2011; Fildani et al., 2013). We propose that this zone of seafloor is an incipient channel developing along a train of cyclic steps which, with ongoing plate convergence and uplift of the continental slope and southeastward migration of the deformation front, would link the mouth of lower Cook Strait Canyon with the Hikurangi channel.

(e) Canyon system state

A channel equilibrium profile is a depth profile created by the erosional and depositional action of gravity flows over a period of thousands of years such that the prevailing sediment discharge is carried through the channel with minimum aggradation or degradation (Pirmez et al., 2000; Ferry et al., 2005). Factors such as the power, frequency and geometry of flows, and the availability of sediment, are the dominant shaping mechanisms that determine the ability of a channel to reach equilibrium (Kneller, 2003). Since the ocean system is not a steady-state system, the channel equilibrium is transient and also dependent on other factors such current regime, slope stability, and strength of near-seafloor sediments (Georgiopoulou and Cartwright, 2013). Topographic steady state, on the other hand, entails a sustained balance between rock uplift and the erosion of the channel (Willgoose et al., 1991; Howard, 1994).

There are many indications that the lower CS is neither in equilibrium nor in a steady state. These include:

(i) Formation and migration of knickpoints (Figure 8), which have been suggested as the dominant mode of channel adjustment in response to a perturbation, and indicate a lack of equilibrium between tectonic and sedimentary processes (Whipple and Tucker, 1999; Crosby and Whipple, 2006).

(ii) The Palliser and Boo Boo Canyon tributaries do not approach the lower Cook Strait Canyon at the same elevation, disobeying Playfair's Law and indicating disequilibrium across the entire canyon system (Playfair, 1802; Niemann et al., 2001).

(iii) The canyons' longitudinal profiles are predominantly linear (Figure 6), which contrasts with the graded profile associated with canyon systems in equilibrium (Gerber et al., 2009; Covault et al., 2011).

(iv) The general lack of canyon-wide, inverse power-law slope-area relationships associated with a spatially equilibrated erosion rate (Figure 11; Whipple, 2004; Wobus et al., 2006).

We therefore consider the lower CS to be in a transient state. The system is undergoing continuous adjustment to perturbations associated with tectonic displacements, base level changes and varying sediment fluxes. These perturbations dominate over the capacity of sedimentary flows to establish an equilibrium profile and topographic steady state.

6.2 TECTONIC INFORMATION FROM CANYON MORPHOLOGY

We use canyon morphology to extract information on two aspects of tectonic activity across the Cook Strait:

(i) Faulting: The MCS data show that few fault tips actually propagate to the seafloor. Single event displacements on these faults may be high (e.g. 10 m

732 across the lower Cook Strait Canyon, as in Figure 3a); however, the
733 uppermost tip of the fault is buried by several hundred meters of folded but
734 unbroken sedimentary sequences. The response of the canyon floor to faulting
735 is thus a localized upward flexure of up to several meters. By analyzing the
736 canyon longitudinal profiles (Figure 7), we are able to propose four new sites
737 where unmapped faults, not identified in the MCS data, may have caused
738 localized upward flexure. All of these sites comprise prolongations of already
739 known faults across the canyon floor, and include the Wairarapa fault across
740 Nicholson Canyon, the Opouawe-Uruti fault at step 17 and another in the
741 lower reaches of Opouawe Canyon, and a fault in the upper reaches of the
742 lower Cook Strait Canyon.
743 (ii) Uplift and incision patterns: The steepest canyon thalweg slope gradients are
744 recorded in Boo Boo, Campbell, Palliser and Opouawe Canyons (Figures 7,
745 12; Table 2). The highest relief, and the canyon segments with lowest R^2 and
746 highest concavity index values in the slope-area regression models, occur in
747 lower Cook Strait, Boo Boo, Campbell, Palliser and Opouawe Canyons
748 (Figures 5b, 12; Table 2). This indicates that the slopes hosting the lower
749 canyons have been undergoing more pronounced rates of uplift and shortening
750 than those hosting the upper canyons, as confirmed by Figures 2 and 4
751 (Whipple and Tucker, 1999; Snyder et al., 2000; Kirby and Whipple, 2001;
752 Wobus et al., 2006; Cowie et al., 2008).
753

6.3 A MODEL FOR CANYON DEVELOPMENT IN RESPONSE TO TECTONIC FORCING

The schematic in Figure 13 summarizes the reported results in a generalized model of canyon geomorphic evolution in tectonically-active continental margins. The model is based on the following:

a. Thrust and strike-slip faults control canyon location and planform shape, in particular width, sinuosity, and dendritic network patterns.

b. Uplift due to folds and/or faults results in:

   (i) Linear to convex thalweg longitudinal profiles;

   (ii) Abrupt changes in, and high values of, slope gradient;

   (iii) Canyon wall asymmetry;

   (iv) Dense gully erosion;

   (v) Hanging valleys at canyon confluences;

   (vi) Slope-area plots with low R^2 values; where not affecedt by faults or knickpoints, the slope-area plots have high R^2 values for inverse power relationships.

c. Seismicity is a main trigger of slope instability across canyon walls, which are preconditioned by undercutting from canyon incision and are responsible for canyon elongation and widening. Seismicity is also associated with higher and more frequent sedimentary flows along the canyon thalweg.

d. Two types of knickpoint develop:

(i) Gentle and rounded knickpoint formed by folds or fault break outs that diffuses by upstream erosion and downstream deposition;

(ii) Steep and angular knickpoints, which are driven by base level lowering (due to regional uplift or deepening of downstream canyons) or changing sediment fluxes, and which migrate upslope by canyon floor slope failures and localized quarrying/plucking; the knickpoint migration rate is a function of the canyon area and the associated sedimentary flow throughput.

Future work will focus on refining the quantitative relationship between canyon morphometric parameters and tectonic processes to enable the direct extraction of quantitative tectonic information from morphology.

7. CONCLUSIONS

Tectonic activity, in the form of major faults and structurally-generated tectonic ridges, leaves a clear topographic signature on submarine canyon location and morphology in the Cook Strait canyon system (CS), Hikurangi Margin off New Zealand's North Island, in particular their dendritic and sinuous planform shapes, steep and linear longitudinal profiles, and canyon wall asymmetry and width. We also report breaks/changes in canyon longitudinal slope profiles and mean slope gradient, relief and slope-area regression models at the intersection with faults.

799 Across the CS we observe two types of knickpoints related to tectonic activity. The first
800 type consists of low slope gradient knickpoints that are rounded and diffusive, forming as
801 a result of short wavelength folds or fault break outs and being restored to an equilibrium
802 profile by upstream erosion and downstream deposition. The second, more widespread
803 type of knickpoints have high slope gradients and angular profiles. These knickpoints
804 have undergone upslope advective migration through slope failures on the canyon floor
805 and localized quarrying and plucking by sedimentary flows. The migration is driven by
806 base level lowering due to multiple episodes of regional uplift of the margin and
807 deepening of lower Cook Strait Canyon floor by sedimentary flows, or by changing
808 sediment fluxes. Variation in lithological resistance is likely to play a secondary and
809 localized role in knickpoint formation and evolution. The stream erosion model is
810 applicable to CS, and knickpoint migration is faster in the larger canyons. The formation
811 and migration of knickpoints, the non-adherence to Playfair's Law, the linear longitudinal
812 profiles and the lack of canyon-wide, inverse power-law slope-area relationships indicate
813 that CS is a system that is neither in topographic steady state nor in equilibrium, and that
814 it is undergoing continuous adjustments to perturbations associated with tectonic
815 displacement and changes in base level and sediment fluxes.
816
817 Canyon morphology also allows us to infer tectonic activity across the CS. From the
818 canyon longitudinal profiles we can propose four new sites in Nicholson, Opouawe and
819 lower Cook Strait Canyons where unmapped prolongations of known faults have caused
820 localized upward flexure. The occurrence in the lower canyons of steep thalweg slope
821 gradients, high relief, and low values of R^2 in the slope-area regression models, and their

822 spatial association with faults and steps, indicate that the lower slopes have undergone
823 more pronounced rates of uplift and shortening than those hosting the upper canyons.
824
825 The reported canyon morphological parameters and their response to tectonic activity
826 allow us to propose a generalised model for canyon geomorphic evolution in tectonically-
827 active continental margins.
828
829 **8. ACKNOWLEDGMENTS**
830
831 This research was undertaken with funding from Marie Curie Intra-European Fellowship
832 PIEF-GA-2009-252702 and Marie Curie Career Integration Grant PCIG13-GA-2013-
833 618149 within the 7th European Community Framework Programme, NIWA under
834 Coasts and Oceans Research Programme 2013/14 and the Royal Society of New Zealand
835 International Mobility Fund contract ISATB09-37. We are indebted to Shanaka de Silva,
836 David J.W. Piper, Neil C. Mitchell and Atsushi Noda for their insightful reviews. Emma
837 Cassar is thanked for her assistance with GIS analysis.
838
839

840 **References**

841

842 Adeogba, A.A., McHargue, T.R., and Graham, S.A., 2005, Transient fan architecture and
843 depositional controls from near-surface 3-D seismic data, Niger Delta continental
844 slope: American Association of Petroleum Geologists Bulletin, v. 89, p. 626-643.
845 Allen, S.E., and Durrieu de Madron, X., 2009, A review of the role of submarine canyons
846 in deep-ocean exchange with the shelf: Ocean Science, v. 5, p. 607-620.
847 Alves, T.M., Strasser, M., and Moore, G.F., in press, Erosional features as indicators of
848 thrust fault activity (Nankai Trough, Japan): Marine Geology.
849 Amblas, D., Gerber, T.P., Canals, M., Pratson, L.F., Urgeles, R., Lastras, G., and Calafat,
850 A., 2011, Transient erosion in the Valencia Trough turbidite systems, NW
851 Mediterranean Basin: Geomorphology, v. 130, p. 173-184.
852 Ansell, J.H., and Bannister, S.C., 1996, Shallow morphology of the subducted Pacific
853 Plate along the Hikurangi Margin, New Zealand: Physics of the Earth and
854 Planetary Interior, v. 93, p. 3-20.
855 Augustin, J.M., and Lurton, X., 2005, Image amplitude calibration and processing for
856 seafloor mapping sonars, Proceedings of the Oceans 2005: London, p. 698-701.
857 Barnes, P.M., and Audru, J.C., 1999a, Quaternary faulting in the offshore Flaxbourne and
858 Wairarapa Basins, southern Cook Strait, New Zealand: New Zealand Journal of
859 Geology and Geophysics, v. 42, p. 349-367.
860 —, 1999b, Recognition of active strike-slip faulting from high-resolution marine seismic
861 reflection profiles: Eastern Marlborough fault system, New Zealand: Geological
862 Society of America Bulletin, v. 111, p. 538-559.

863 Barnes, P.M., Lamarche, G., Bialas, J., Pecher, I., Henrys, S., Netzeband, G., Greinert, J.,
864 Mountjoy, J.J., Pedley, K., and Crutchley, G.J., 2010, Tectonic and geological
865 framework for gas hydrates and cold seeps on the Hikurangi subduction margin,
866 New Zealand: Marine Geology, v. 272, p. 26-48.
867 Barnes, P.M., and Mercier de Lepinay, B., 1997, Rates and mechanics of rapid frontal
868 accretion along the very obliquely convergent southern Hikurangi margin, New
869 Zealand: Journal of Geophysical Research, v. 102, p. 24931-24952.
870 Barnes, P.M., Mercier de Lepinay, B., Collot, J.Y., Delteil, J., and Audra, J.C., 1998,
871 Strain partitioning in the transition area between oblique subduction and
872 continental collision, Hikurangi Margin, New Zealand: Tectonics, v. 17, p. 534-
873 557.
874 Beavan, J., Tregoning, P., Bevis, M., Kato, T., and Meertens, C., 2002, Motion and
875 rigidity of the Pacific Plate and implications for plate boundary deformation:
876 Journal of Geophysical Research - Solid Earth, v. 107, p. 2261.
877 Berryman, K., Marden, M., Palmer, A., Wilson, K., Mazengarb, C., and Litchfield, N.,
878 2010, The post-glacial downcutting history in the Waihuka tributary of Waipaoa
879 River, Gisborne district: Implications for tectonics and landscape evolution in the
880 Hikurangi subduction margin, New Zealand: Marine Geology, v. 270, p. 55-71.
881 Bishop, P., 2007, Long-term landscape evolution: Linking tectonic and surface processes:
882 Earth Surface Processes and Landforms, v. 32, p. 329-365.
883 Bishop, P., Hoey, T.B., Jansen, J.D., and Artza, I.L., 2005, Knickpoint recession rate and
884 catchment area: The case of uplifted rivers in eastern Scotland: Earth Surface
885 Processes and Landforms, v. 30, p. 767-778.

886 Brocklehurst, S.H., 2010, Tectonics and geomorphology: Progress in Physical
887 Geography, v. 34, p. 357-383.
888 Brothers, D.S., Ten Brink, U.S., Andrews, B.D., Chaytor, J.D., and Twichell, D.C., 2013,
889 Geomorphic process fingerprints in submarine canyons: Marine Geology, v. 337,
890 p. 53-66.
891 Burbank, D.W., Leland, J., Fielding, E., Anderson, R.S., Brozovic, N., Reid, M.R., and
892 Duncan, C., 1996, Bedrock incision, rock uplift and threshold hillslopes in the
893 northwestern Himalayas: Nature, v. 379, p. 505-510.
894 Canals, M., Company, J.B., Martin, D., Sanchez-Vidal, A., and Ramirez-Llodra, E.,
895 2013, Integrated study of Mediterranean deep sea canyons: Novel results and
896 future challenges: Progress in Oceanography, v. 118, p. 1-27.
897 CANZ, 2008, New Zealand Region Bathymetry, 1:4 000 000: Wellington, New Zealand,
898 National Institute of Water and Atmospheric Research.
899 Carter, L., Wright, I.C., Collins, N., Mitchell, J.S., and Win, G., 1991, Seafloor stability
900 along the Cook Strait power cable corridor, 10th Australian Conference on
901 Coastal and Ocean Engineering, p. 565-570.
902 Carter, R.M., 1988, The nature and evolution of deep-sea channel systems: Basin
903 Research, v. 1, p. 41-54.
904 Cartigny, M.J.B., Postma, G., van den Berg, J.H., and Mastbergen, D.R., 2011, A
905 comparative study of sediment waves and cyclic steps based on geometries,
906 internal structures and numerical modeling: Marine Geology, v. 280, p. 40-56.

907 Chiang, S.H., and Yu, H.S., 2006, Morphotectonics and incision of the Kaoping
908 submarine canyon, SW Taiwan orogenic wedge: Geomorphology, v. 80, p. 199-
909 213.
910 Clark, K.J., Hayward, B.W., Cochran, U.A., Grenfell, H.R., Hemphill–Haley, E.,
911 Mildenhall, D.C., Hemphill–Haley, M.A., and Wallace, L.M., 2011, Investigating
912 subduction earthquake geology along the southern Hikurangi margin using
913 palaeoenvironmental histories of intertidal inlets: New Zealand Journal of
914 Geology and Geophysics, v. 54, p. 255-271.
915 Covault, J.A., Fildani, A., Romans, B.W., and McHargue, T., 2011, The natural range of
916 submarine canyon-and-channel longitudinal profiles: Geosphere, v. 7, p. 313-332.
917 Cowie, P.A., Whittaker, A.C., Attal, M., Roberts, G., Tucker, G.E., and Ganas, A., 2008,
918 New constraints on sediment-flux-dependent river incision: Implications for
919 extracting tectonic signals from river profiles: Geology, v. 36, p. 535-538.
920 Crosby, B.T., and Whipple, K.X., 2006, Knickpoint initiation and distribution within
921 fluvial networks: 236 waterfalls in the Waipoa River, North Island, New Zealand:
922 Geomorphology, v. 82, p. 16-38.
923 Dadson, S.J., Hovius, N., Chen, H., Dade, W.B., Lin, J.C., Hsu, M.L., Lin, C.W., Horng,
924 M.J., Chen, T.C., and Milliman, J., 2004, Earthquake-triggered increase in
925 sediment delivery from an active mountain belt: Geology, v. 32, p. 733-736.
926 Demoulin, A., 1998, Testing the tectonic significance of some parameters of longitudinal
927 river profiles: The case of the Ardenne (Belgium, NW Europe): Geomorphology,
928 v. 24, p. 189-208.

929 Estrada, F., Ercilla, G., and Alonso, B., 2005, Quantitative study of a Magdalena
930 submarine channel (Caribbean Sea): Implications for sedimentary dynamics:
931 Marine and Petroleum Geology, v. 22, p. 623-635.
932 Farre, J.A., McGregor, B.A., Ryan, W.B.F., and Robb, J.M., 1983, Breaching the
933 shelfbreak: Passage from youthful to mature phase in submarine canyon
934 evolution: Society of Economic Paleontologists and Mineralogists, Special
935 Publication, v. 33, p. 25-39.
936 Ferry, J.N., Mulder, T., Parize, O., and Raillard, S., 2005, Concept of equilibrium profile
937 in deep-water turbidite systems: Effects of local physiographic changes on the
938 nature of sedimentary processes and the geometries of deposits, *in* Hodgson,
939 D.M., and Flint, S.S., eds., Submarine Slope Systems: Processes and Products,
940 Volume 244: London, Geological Society, p. 181-193.
941 Fildani, A., Hubbard, S.M., Covault, J.A., Maier, K.L., Romans, B.W., Traer, M., and
942 Rowland, J.C., 2013, Erosion at inception of deep-sea channels: Marine and
943 Petroleum Geology, v. 41, p. 48-61.
944 Fildani, A., Normark, W.R., Kostic, S., and Parker, G., 2006, Channel formation by flow
945 stripping: Large-scale scour features along the Monterey East Channel and their
946 relation to sediment waves: Sedimentology, v. 53, p. 1265-1287.
947 Flint, J.J., 1974, Stream gradient as a function of order, magnitude and discharge: Water
948 Resources Research, v. 10, p. 969-973.
949 Fraser, S., Power, W., Wang, X., Wallace, L., Mueller, C., and Johnston, D., 2014,
950 Tsunami inundation in Napier, New Zealand, due to local earthquake sources:
951 Natural Hazards, v. 70, p. 415-445.

952 Georgiopoulou, A., and Cartwright, J.A., 2013, A critical test of the concept of submarine
953 equilibrium profile: Marine and Petroleum Geology, v. 41, p. 35-47.
954 Geotrace, 2010, Pegasus, Bounty Trough, Great South Basin and Sahke Processing
955 Report, *in* Ministry of Economic Development New Zealand Unpublished
956 Petroleum Report, ed.
957 Gerber, T.P., Amblas, D., Wolinsky, M.A., Pratson, L.F., and Canals, M., 2009, A model
958 for the long-profile shape of submarine canyons: Journal of Geophysical
959 Research, v. 114, p. F03002.
960 Grapes, R.H., and Downes, G., 1997, The 1885 Wairarapa, New Zealand, earthquake -
961 Analysis of historical data: Bulletin of the New Zealand Society for Earthquake
962 Engineering, v. 30, p. 271-369.
963 Grapes, R.H., Little, T.A., and Downes, G., 1998, Rupturing on the Awatare Fault during
964 the 1848 October Marlborough earthquake, New Zealand: Historical and present
965 day evidence: New Zealand Journal of Geology and Geophysics, v. 41, p. 387-
966 399.
967 Greene, H.G., Maher, D., and Paull, C.K., 2002, Physiography of the Monterey Bay
968 National Marine Sanctuary and implications about continental margin
969 development: Marine Geology, v. 181, p. 55-82.
970 Harris, P.T., and Whiteway, T., 2011, Global distribution of large submarine canyons:
971 Geomorphic differences between active and passive continental margins: Marine
972 Geology, v. 285, p. 69-86.

973 Heiniö, P., and Davies, R.J., 2007, Knickpoint migration in submarine channels in
974 response to fold growth, western Niger Delta: Marine and Petroleum Geology, v.
975 24, p. 434-449.
976 Henrys, S., Wech, A., Sutherland, R., Stern, T., Savage, M., Sato, H., Mochizuki, K.,
977 Iwasaki, T., Okaya, D., Seward, A., Tozer, B., Townend, J., Kurashimo, E.,
978 Iidaka, T., and Ishiyama, T., 2013, SAHKE geophysical transect reveals crustal
979 and subduction zone structure at the southern Hikurangi margin, New Zealand:
980 Geochemistry, Geophysics, Geosystems, v. 14, p. 2063-2083.
981 Howard, A.D., 1994, A detachment-limited model of drainage basin evolution: Water
982 Resources Research, v. 30, p. 2261-2285.
983 Howard, A.D., and Kerby, G., 1983, Channel changes in badlands: Geological Society of
984 America Bulletin, v. 94, p. 739-752.
985 Huyghe, P., Foata, M., Deville, E., Mascle, G., and Caramba Working Group, 2004,
986 Channel profiles through the active thrust front of the southern Barbados prism:
987 Geology, v. 32, p. 429-432.
988 Kirby, E., and Whipple, K.X., 2001, Quantifying differential rock-uplift rates via stream
989 profile analysis: Geology, v. 29, p. 415-418.
990 Kneller, B., 1995, Beyond the turbidite paradigm: Physical models for deposition of
991 turbidites and their implications for reservoir prediction, *in* Harley, A.J., and
992 Prosser, D.J., eds., Characterization of deep marine clastic systems, Volume 94:
993 London, Geological Society Special Publications, p. 31-49.
994 —, 2003, The influence of flow parameters on turbidite slope channel architecture:
995 Marine and Petroleum Geology, v. 20, p. 901-910.

996 Kostic, S., 2011, Modeling of submarine cyclic steps: Controls on their formation,
997 migration, and architecture: Geosphere, v. 7, p. 294-304.
998 Kukowski, N., Schillhorn, T., Huhn, K., von Rad, U., Husen, R., and Flueh, E.R., 2001,
999 Morphotectonics and mechanics of the central Makran accretionary wedge off
1000 Pakistan: Marine Geology, v. 173, p. 1-19.
1001 Lamarche, G., Lurton, X., Verdier, A.-L., and Augustin, J.-M., 2011, Quantitative
1002 characterisation of seafloor substrate and bedforms using advanced processing of
1003 multibeam backscatter—Application to Cook Strait, New Zealand: Continental
1004 Shelf Research, v. 31, p. S93-S109.
1005 Laursen, J., and Normark, W.R., 2002, Late Quaternary evolution of the San Antonio
1006 Submarine Canyon in the central Chile forearc (~33°S): Marine Geology, v. 188,
1007 p. 365-390.
1008 Le Dantec, N., Hogarth, L.J., Driscoll, N.W., Babcock, J.M., Barnhardt, W.A., and
1009 Schwab, W.C., 2010, Tectonic controls on nearshore sediment accumulation and
1010 submarine canyon morphology offshore La Jolla, Southern California: Marine
1011 geology, v. 268, p. 115-128.
1012 Lewis, K.B., and Barnes, P.M., 1999, Kaikoura Canyon, New Zealand: Active conduit
1013 from near-shore sediment zones to trench-axis channel: Marine Geology, v. 162,
1014 p. 39-69.
1015 Litchfield, N.J., Van Dissen, R., Sutherland, R., Barnes, P.M., Cox, S.C., Norris, R.,
1016 Beavan, R.J., Langridge, R., Villamor, P., Berryman, K., Stirling, M., Nicol, A.,
1017 Nodder, S., Lamarche, G., Barrell, D.J.A., Pettinga, J.R., Little, T., Pondard, N.,

1018 Mountjoy, J.J., and Clark, K., 2013, A model of active faulting in New Zealand:
1019 New Zealand Journal of Geology and Geophysics, v. 57, p. 32-56.
1020 McSaveney, M.J., Graham, I.J., Begg, J.G., Beu, A.G., Hull, A.G., Kim, K., and
1021 Zondervan, A., 2006, Late Holocene uplift of beach ridges at Turakirae Head,
1022 south Wellington coast, New Zealand: New Zealand Journal of Geology and
1023 Geophysics, v. 49, p. 337-358.
1024 Micallef, A., Berndt, C., Masson, D.G., and Stow, D.A.V., 2007, A technique for the
1025 morphological characterization of submarine landscapes as exemplified by debris
1026 flows of the Storegga Slide: Journal of Geophysical Research, v. 112, p. F02001.
1027 Micallef, A., and Mountjoy, J.J., 2011, A topographic signature of a hydrodynamic origin
1028 for submarine gullies: Geology, v. 39, p. 115-118.
1029 Micallef, A., Mountjoy, J.J., Canals, M., and Lastras, G., 2012, Deep-seated bedrock
1030 landslides and submarine canyon evolution in an active tectonic margin: Cook
1031 Strait, New Zealand., *in* Yamada, Y., Kawamura, K., Ikehara, K., Ogawa, Y.,
1032 Urgeles, R., Mosher, D., Chaytor, J.D., and Strasser, M.C., eds., Submarine Mass
1033 Movements and Their Consequences, Volume 31: London, Springer, p. 201-212.
1034 Miller, J.R., 1991, The influence of bedrock geology on knickpoint development and
1035 channel-bed degradation along downcutting streams in south-central Indiana:
1036 Journal of Geology, v. 99, p. 591-605.
1037 Ministry of Economic Development, 2010, Geotrace, Pegasus, Bounty Trough, Great
1038 South Basin and Sahke processing report: Wellington, Ministry of Economic
1039 Development.

1040 Mitchell, N.C., 1993a, Comment on the mapping of iron-manganese nodule fields using
1041 reconnaissance sonars such as GLORIA: Geo-Marine Letters, v. 13, p. 244-247.
1042 —, 1993b, A model for attenuation of backscatter due to sediment accumulations and its
1043 application to determine sediment thickness with GLORIA sidescan sonar:
1044 Journal of Geophysical Research, v. 98, p. 22477-22493.
1045 —, 2004, Form of submarine erosion from confluences in Atlantic USA continental slope
1046 canyons: American Journal of Science, v. 304, p. 590-611.
1047 —, 2005, Interpreting long-profiles of canyons in the USA Atlantic continental slope:
1048 Marine Geology, v. 214, p. 75-99.
1049 —, 2006, Morphologies of knickpoints in submarine canyons: Geological Society of
1050 America Bulletin, v. 118, p. 589-605.
1051 Mountain, G.S., Damuth, J.E., McHugh, C.M., Lorenzo, J.M., and Fulthorpe, C.S., 1996,
1052 Origin, reburial and signficance of a Middle Miocene canyon, New Jersey
1053 continental slope, *in* Mountain, G.S., Miller, K., Blum, P., Poag, C.W., and
1054 Twichell, D.C., eds., Proceedings of the Ocean Drilling Programme Volume 150:
1055 Texas, Ocean Drilling Programme, p. 283-292.
1056 Mountjoy, J.J., 2013, Cook Strait quakes too small for landslide-tsunami, Water and
1057 Atmosphere, Volume 8: Wellington, NIWA.
1058 Mountjoy, J.J., Barnes, P.M., and Pettinga, J.R., 2009, Morphostructure and evolution of
1059 submarine canyons across an active margin: Cook Strait sector of the Hikurangi
1060 Margin, New Zealand: Marine Geology, v. 260, p. 45-68.

1061 Mountjoy, J.J., Micallef, A., Stevens, C., and Stirling, M., 2013, Holocene activity in a
1062 non-terrestrially-coupled submarine canyon: Cook Strait, New Zealand.: Deep-
1063 Sea Research II, v. in press.
1064 Nagel, S.R., Mullins, H.T., and Greene, H.G., 1986, Ascension Submarine Canyon,
1065 California - Evolution of a multi-head canyon system along a strike-slip
1066 continental margin (USA): Marine Geology, v. 73, p. 285-310.
1067 Niemann, J.D., Gasparaini, N.M., Tucker, G.E., and Bras, R.L., 2001, A quantitative
1068 evaluation of Playfair's law and its use in testing long-term stream erosion
1069 models: Earth Surface Processes and Landforms, v. 26, p. 1317-1332.
1070 Noda, A., Tuzino, T., Furukawa, R., Joshima, M., and Uchida, J., 2008, Physiographical
1071 and sedimentological characteristics of submarine canyons developed upon an
1072 active forearc slope: The Kushiro Submarine Canyon, northern Japan: Geological
1073 Society of America Bulletin, v. 120, p. 750-767.
1074 Normark, W.R., and Carlson, P.R., 2003, Giant submarine canyons: Is size any clue to
1075 their importance in the rock record?: Geological Society of America Special
1076 Paper, v. 370, p. 175-190.
1077 Normark, W.R., and Curray, J.R., 1968, Geology and structure of the tip of Baja
1078 California, Mexico: Geological Society of America Bulletin, v. 79, p. 1589-1600.
1079 Orpin, A.R., 2004, Holocene sediment deposition on the Poverty-slope margin by the
1080 muddy Waipaoa River: East coast New Zealand: Marine Geology, v. 209, p. 69-
1081 90.
1082 Ouchi, S., 1985, Response of alluvial rivers to slow active tectonic movement:
1083 Geological Society of America Bulletin, v. 96, p. 504-515.

1084 Paola, C., 2000, Quantitative models in sedimentary basin filling: Sedimentology, v. 47,
1085 p. 121-178.
1086 Parker, G., and Izumi, N., 2000, Purely erosional cyclic and solitary steps created by flow
1087 over a cohesive bed: Journal of Fluid Mechanics, v. 419, p. 203-238.
1088 Paull, C.K., Caress, D.W., Ussler, W., Lundsten, E., and Meiner-Johnson, M., 2011,
1089 High-resolution bathymetry of the axial channels within Monterey and Soquel
1090 submarine canyons, offshore central California: Geosphere, v. 7, p. 1077-1101.
1091 Phillips, J.D., McCormack, S., Duan, J., Russo, J.P., Schumacher, A.M., Tripathi, G.N.,
1092 Brockman, R.B., Mays, A.B., and Pulugurtha, S., 2010, Origin and interpretation
1093 of knickpoints in the Big South Fork River basin, Kentucky-Tennessee:
1094 Geomorphology, v. 114, p. 188-198.
1095 Pirmez, C., Beaubouef, R.T., Friedmann, S.J., and Mohrig, D.C., 2000, Equilibrium
1096 profile and baselevel in submarine channels: Examples from Late Pleistocene
1097 systems and implications for the architecture of deep water reservoirs, *in* Weimar,
1098 P., Slatt, R.M., Coleman, J.M., Rosen, N.C., Nelson, H., Bouma, A.H., Styzen,
1099 M.J., and Lawrence, D.T., eds., Deep Water Reservoirs of the World, GCSSEPM
1100 Foundation 20th Annual Research Conference, p. 782-805.
1101 Playfair, J., 1802, Illustrations of the Huttonian Theory of the Earth: London, Cadell and
1102 Davies.
1103 Plaza-Faverola, A., Klaeschen, D., Barnes, P., Pecher, I., Henrys, S., and Mountjoy, J.J.,
1104 2012, Evolution of fluid expulsion and concentrated hydrate zones across the
1105 southern Hikurangi subduction margin, New Zealand: An analysis from depth
1106 migrated seismic data: Geochemistry, Geophysics, Geosystems, v. 13, p. Q08018.

1107 Pondard, N., and Barnes, P.M., 2010, Structure and paleoearthquake records of active
1108 submarine faults, Cook Strait, New Zealand: Implications for fault interactions,
1109 stress loading, and seismic hazard: Journal of Geophysical Research, v. 115, p.
1110 B12320.
1111 Pratson, L.F., and Coakley, B.J., 1996, A model for the headward erosion of submarine
1112 canyons induced by downslope-eroding sediment flows: Geological Society of
1113 America Bulletin, v. 108, p. 225-234.
1114 Pratson, L.F., Imran, J., Parker, G., Syvitski, J.P., and Hutton, E.H., 2000, Debris flows
1115 vs. turbidity currents: A modelling comparison of their dynamics and deposits, *in*
1116 Bouma, A.H., and Stone, C.G., eds., Fine-grained Turbidite Systems, Volume 68,
1117 American Association of Petroleum Geologists Memoir, p. 57-72.
1118 Pratson, L.F., Nittrouer, C.A., Wiberg, P.L., Steckler, M.S., Swenson, J.B., Cacchione,
1119 D.A., Karson, J.A., Murray, A.B., Wolinsky, M.A., Gerber, T.P., Mullenbach,
1120 B.L., Spinelli, G.A., Fulthorpe, C.S., O'Grady, D.B., Parker, G., Driscoll, N.W.,
1121 Burger, R.L., Paola, C., Orange, D.L., Field, M.E., Friedrichs, C.T., and Fedele,
1122 J.J., 2009, Seascape evolution on clastic continental shelves and slopes, *in*
1123 Nittrouer, C.A., Austin, J.A., Field, M.E., Kravitz, J.H., Syvitski, J.P.M., and
1124 Wiberg, P.L., eds., Continental Margin Sedimentation: From Sediment Transport
1125 to Sequence Stratigraphy: IAP Special Publication, Volume 37: Oxford,
1126 Blackwell Publishing, p. 339-380.
1127 Pratson, L.F., Ryan, W.B.F., Mountain, G.S., and Twichell, D.C., 1994, Submarine
1128 canyon initiation by downslope-eroding sediment flows: Evidence in late

1129 Cenozoic strata on the New Jersey continental slope: Geological Society of
1130 America Bulletin, v. 106, p. 395-412.
1131 Ramsey, L.A., Hovius, N., Lague, D., and Liu, C.S., 2006, Topographic characteristics of
1132 the submarine Taiwan orogen: Journal of Geophysical Research, v. 111, p.
1133 F02009.
1134 Shepard, F.P., 1981, Submarine canyons: Multiple causes and long-time persistence:
1135 American Association of Petroleum Geologists Bulletin, v. 65, p. 1062-1077.
1136 Snyder, N.P., Whipple, K.X., Tucker, G.E., and Merritts, D.J., 2000, Landscape response
1137 to tectonic forcing: Digital elevation model analysis of stream profiles in the
1138 Mendocino triple junction region, northern California: Geological Society of
1139 America Bulletin, v. 112, p. 1250-1263.
1140 —, 2003, Channel response to tectonic forcing: Field analysis of stream morphology and
1141 hydrology in the Mendocino triple junction region, northern California:
1142 Geomorphology, v. 53, p. 97-127.
1143 Soh, W., and Tokuyama, H., 2002, Rejuvenation of submarine canyon associated with
1144 ridge subduction, Tenryu Canyon, off Tokai, central Japan: Marine Geology, v.
1145 187, p. 203-220.
1146 Sougnez, N., and Vanacker, V., 2011, The topographic signature of Quaternary tectonic
1147 uplift in the Ardennes massif (Western Europe): Hydrology and Earth System
1148 Sciences, v. 15, p. 1095-1107.
1149 Stevens, C.L., Smith, M.J., Grant, B., Stewart, C.L., and Divett, T., 2012, Tidal energy
1150 resource complexity in a large strait: The Karori Rip, Cook Strait: Continental
1151 Shelf Research, v. 33, p. 100-109.

1152 Stirling, M.W., McVerry, G., Gersenberger, M., Litchfield, N., Van Dissen, R.,
1153 Berryman, K., Barnes, P.M., Wallace, L., Villamor, P., Langridge, R., Lamarche,
1154 G., Nodder, S., Reyners, M., Bradley, B., Rhoades, D., Smith, W., Nicol, A.,
1155 Pettinga, J.R., Clark, K., and Jacobs, K., 2012, National seismic hazard model for
1156 New Zealand: 2010 update: Bulletin of the Seismological Society of America, v.
1157 102, p. 1514-1542.
1158 Straub, K.M., Jerolmack, D.J., Mohrig, D., and Rothman, D.H., 2007, Channel network
1159 scaling laws in submarine basins: Geophysical Research Letters, v. 34, p. L12613.
1160 Sultan, N., Cochonat, P., Canals, M., Cattaneo, A., Dennielou, B., Haflidason, H.,
1161 Laberg, J.S., Long, D., Mienert, J., Trincardi, F., Urgeles, R., Vorren, T.O., and
1162 Wilson, C., 2004, Triggering mechanisms of slope instability processes and
1163 sediment failures on continental margins: a geotechnical approach: Marine
1164 Geology, v. 213, p. 291-321.
1165 Sultan, N., Gaudin, M., Berne, S., Canals, M., Urgeles, R., and Lafuerza, S., 2007,
1166 Analysis of slope failure in submarine canyon heads: An example from the Gulf
1167 of Lions: Journal of Geophysical Research, v. 112, p. F01009.
1168 Toniolo, H., and Cantelli, A., 2007, Experiments on upstream-migrating submarine
1169 knickpoints: Journal of Sedimentary Research, v. 77, p. 772-783.
1170 Tubau, X., Lastras, G., Canals, M., Micallef, A., and Amblas, D., 2013, Significance of
1171 the fine drainage pattern for submarine canyon evolution: The Foix Canyon
1172 system, northwestern Mediterranean Sea.: Geomorphology, v. 184, p. 20-37.
1173 Turmel, D., Locat, J., and Parker, G., 2011, Upstream migration of knickpoints:
1174 Geotechnical considerations, *in* Yamada, Y., Kawamura, K., Ikehara, K., Ogawa,

1175 Y., Urgeles, R., Mosher, D., Chaytor, J.D., and Strasser, M.C., eds., Submarine
1176 Mass Movements and Their Consequences, Volume 31: London, Springer, p.
1177 123-132.
1178 Twichell, D.C., and Roberts, D.G., 1982, Morphology, distribution and development of
1179 submarine canyons on the United States Atlantic continental slope between
1180 Hudson and Baltimore Canyons: Geology, v. 10, p. 408-412.
1181 Uruski, C.I., 2010, New Zealand's deepwater frontier: Marine and Petroleum Geology, v.
1182 27, p. 2005-2026.
1183 Vachtman, D., Mitchell, N.C., and Gawthorpe, B., 2013, Morphologic signatures in
1184 submarine canyons and gullies, central USA Atlantic continental margins: Marine
1185 and Petroleum Geology, v. 41, p. 250-263.
1186 Wallace, L., Barnes, P., Beavan, J., Van Dissen, R., Litchfield, N., Mountjoy, J.,
1187 Langridge, R., Lamarche, G., and Pondard, N., 2012, The kinematics of a
1188 transition from subduction to strike-slip: An example from the central New
1189 Zealand plate boundary: Journal of Geophysical Research, v. 117, p. B02405.
1190 Wallace, L.M., Beavan, J., McCaffrey, R., and Darby, D., 2004, Subduction zone
1191 coupling and tectonic block rotations in the North Island, New Zealand: Journal
1192 of Geophysical Research, v. 109, p. B12406.
1193 Whipple, K.X., 2004, Bedorck rivers and the geomorphology of active orogens: Annual
1194 Review of Earth and Planetary Sciences, v. 32, p. 151-185.
1195 —, 2009, The influence of climate on the tectonic evolution of mountain belts: Nature
1196 Geoscience, v. 2, p. 97-104.

1197 Whipple, K.X., and Tucker, G.E., 1999, Dynamics of the stream-power river incision
1198 model: Implications for height limits of mountain ranges, landscape response
1199 timescales, and research needs: Journal of Geophysical Research, v. 104, p.
1200 17661-17674.
1201 —, 2002, Implications of sediment-flux-dependent river incision models for landscape
1202 evolution: Journal of Geophysical Research, v. 107.
1203 Whittaker, A.C., Attal, M., Cowie, P.A., Tucker, G.E., and Roberts, G., 2008, Decoding
1204 temporal and spatial patterns of fault uplift using transient river long profiles:
1205 Geomorphology, v. 100, p. 506-526.
1206 Willgoose, G., Bras, R.L., and Rodriguez-Iturbe, I., 1991, A coupled channel network
1207 growth and hillslope evolution model. 1. Theory: Water Resources Research, v.
1208 27, p. 1671-1684.
1209 Wobus, C., Whipple, K.X., Kirby, E., Snyder, N., Johnson, J., Spyropolou, K., Crosby,
1210 B., and Sheehan, D., 2006, Tectonics from topography: Procedures, promise and
1211 pitfalls, *in* Willett, S.D., Hovius, N., Brandon, M.T., and Fisher, D.M., eds.,
1212 Tectonics, Climate, and Landscape Evolution: Geological Society of America
1213 Special Paper 398, Penrose Conference Series, p. 55-74.
1214 Yanites, B.J., Tucker, G.E., Mueller, K.J., and Chen, Y.C., 2010, How rivers react to
1215 large earthquakes: Evidence from central Taiwan: Geology, v. 38, p. 639-642.
1216
1217

Tables

Table 1: Morphometrics of the Cook Strait canyon system (CS).

Canyon	Nicholson	Cook Strait		Wairarapa	Boo Boo	Pallisr	Opouawe	Campbell
		upper	lower					
Length (km)	21.3	50.3	79.0	36.0	12.1	22.7	58.1	47.5
Maximum width (km)	8.9	12.7	14.8	10.7	5.6	11.9	13.7	12.0
Depth from canyon head to mouth (m)	600	1000	1400	1000	1200	1600	2200	2200
General orientation	NW-SE	NW-SE	N-S	NE-SW	W-E	NE-SW	NE-SW	NW-SE
Area (km^2)	113	386	436	320	35	166	465	182
Mean thalweg slope gradient (°)	1.28	1.07	1.25	1.28	5.74	3.09	2.08	3.18
Landslide density (km^{-1})	0.0976	0.233	0.082	0.1327	0	0.1947	0.066	0.054
Gully density (km^{-1})	0.67	0.27	0.81	0.51	2.37	0.86	1.12	0.95
Maximum relief (m)	330	440	1200	450	640	600	640	560

1239 Table 2: Step and depression morphometrics.

Label	Type	Bathymetric depth (m)	Canyon	Height (m)	Gradient (°)	Extension
1	step	717	Nicholson	20	8.8	narrow
2	step	1033	Wairarapa	71	24.3	canyon width
3	step	1147	upper Cook Strait	21	6.8	narrow
4	step	1253	lower Cook Strait	33	2.3	narrow
5	step	1354	lower Cook Strait	54	13.9	canyon width
6	step	1396	lower Cook Strait	47	7.3	narrow
7	step	1340	Boo Boo	50	18.6	narrow
8	step	1256	Boo Boo	68	30.0	narrow
9	step	1199	Boo Boo	79	29.8	narrow
10	step	1065	Boo Boo	98	29.0	canyon width
11	step	816	Boo Boo	233	31.2	canyon width
12	step	1542	Palliser	125	25.7	canyon width
13	step	1483	Palliser	31	10.8	canyon width
14	step	1391	Palliser	28	9.0	narrow
15	step	1286	Palliser	88	19.0	canyon width
16	step	589	Palliser	59	26.4	canyon width
17	step	1499	Opouawe	21	6.7	narrow
18	step	1850	Opouawe	49	8.5	narrow
19	step	1917	Opouawe	115	19.2	canyon width
20	step	508	Campbell	85	31.6	canyon width
21	step	719	Campbell	32	28.5	canyon width
22	step	972	Campbell	114	34.8	canyon width
23	step	1400	Campbell	38	21.0	narrow
24	step	1995	Campbell	74	14.4	narrow
25	step	2149	Campbell	78	13.4	narrow
26	step	2217	Campbell	165	22.0	canyon width
27	step	2383	lower Cook Strait	58	8.1	narrow

28	step	2495	Opouawe	49	9.4	narrow
29	depression	2507	lower Cook Strait	120	6.8	narrow
30	depression	2538	lower Cook Strait	50	4.1	narrow
31	depression	2609	lower Cook Strait	60	11.3	narrow
32	depression	2639	lower Cook Strait	50	9.5	narrow
33	depression	2686	lower Cook Strait	25	4.8	narrow
34	depression	2683	lower Cook Strait	55	5.7	narrow
35	depression	2694	lower Cook Strait	30	3.4	narrow
36	depression	2687	lower Cook Strait	20	3.8	narrow

Figure captions

Figure 1: Location map (inset) and shaded relief bathymetric map of Cook Strait with main structural elements of the southern Hikurangi margin (angle of illumination is NW). The borders of the submarine canyons are denoted by white polygons. The black triangles indicate the direction of the thrust faults. The dashed dark red lines represent the continental shelf break. The Hikurangi channel in the inset is denoted by 'HC'.

Figure 2: a) Depth-migrated regional multichannel seismic reflection (MCS) profile Pegasus09-19 illustrating the active plate interface between the subducting Pacific Plate and the overlying Australian Plate (modified from Plaza-Faverola et al. (2012)). Active faults in the upper plate are deforming the continental slope and forming ridges (e.g. Opouawe Bank) that have a controlling influence on slope morphology. Location shown in figure 1. Acronyms: BSR (Bottom Simulating Reflector), O-UF (Opouawe-Uruti fault), PF (Pahaua fault), MES (late Cretaceous sequence), LIP (lithospheric plate). b) Enlargement of the part of the MSC profile illustrating the shallow details of active fault tips as they approach the seabed. Green arrows are indicative of old canyons/channels that have subsequently been infilled.

Figure 3: a) Active faulting and ground shaking. Background color stretch shows the peak ground acceleration in pga expected for a return period of 1000 years. The red lines represent the seismic sources in the probabilistic seismic hazard model used to generate the ground shaking levels and the associated values show the range of Single Event

1263 Displacements expected for each fault (after Stirling et al. (2012)). b) The Hikurangi
1264 subduction zone beneath Cook Strait. Blue contours show the depth of the subduction
1265 interface (after Ansell and Bannister, (1996)). White contours and green to red color
1266 stretch show the predicted uplift of the seafloor for a full rupture of the Hikurangi
1267 subduction thrust (after Fraser et al. (2014)).
1268
1269 Figure 4: a) Time-migrated MCS reflection profile Pegasus09-15 illustrating the actively
1270 propagating folds beneath lower Cook Strait Canyon. Stratigraphy after Plaza-Faverola et
1271 al. (2012). Location shown in figure 1. b) Enlargement of profile illustrating the blind
1272 fault tips beneath the canyon, and erosion of stratigraphy within the canyon.
1273
1274 Figure 5: Maps of (a) acoustic backscatter, (b) relief, (c) landslide scars and (d) gullies
1275 across the Cook Strait canyon system (CS).
1276
1277 Figure 6: Normalized canyon longitudinal profiles of all CS canyons.
1278
1279 Figure 7: Longitudinal profile maps of all canyons in CS denoting locations of faults
1280 known from seismic reflection data (in red), new faults mapped from morphological data
1281 (in purple), steps (in blue), and depressions (in green). The black dashed lines on maps
1282 locate canyon thalwegs. Bathymetric maps with isobaths (20 m interval) are shown for
1283 step 1 (figure a) – step 1 in Nicholson Canyon floor coincides with channelized
1284 morphology located to the SW of a 70 m high escarpment associated to the Wharekauhau
1285 fault; step 2 (figure b) - double arcuate scar on Wairarapa Canyon floor with ridge below;

steps 12-15 (figure d) – four crescent-shaped scars on the Palliser Canyon floor with similarly shaped scars across the canyon walls; steps 7-11 (figure e) – a series of five crescent-shaped scars on the Boo Boo Canyon floor, with step 11 comprising the highest step (233 m) across the entire CS; depressions 29-36 (figure h) – a series of upslope-asymmetric depressions downstream of the mouth of lower Cook Strait Canyon. DTIS imagery from transect 31 downslope of step 4 is shown in figure h; the location of this transect is shown in figure 8. The location of figures 7a, 7b, 7d, 7e and 7h is shown in figure 8.

Figure 8: Map of steps and depressions across the CS.

Figure 9: Bar chart of the distance of selected steps from the local base level (floor of lower Cook Strait Canyon). The step number is denoted in bold and italics. Steps that have similar distances are denoted by same bar color.

Figure 10: Plot of canyon area against the distance of steps from the local base level (measured from either the regional base level or the floor of the canyon in which the canyon hosting the step drains), for lower canyons.

Figure 11: Thalweg slope-area plots for all canyons in the CS. A dashed black line in each plot represents a moving average estimated for all points in the plot. The moving average was used to divide the plot into segments (denoted by differently coloured points). Regression analyses were carried out to determine the regression model for slope

and area (power law; dark grey solid line), the coefficient of determination (R^2), and the mean of the slope values (x) for each segment. Where possible, the boundaries between segments are associated with fault or steps.

Figure 12: Map of slope-area segments for each canyon shaded according to the mean slope gradient.

Figure 13: Summary model illustrating modes of canyon response to active tectonic processes.

Figure 1
Click here to download high resolution image

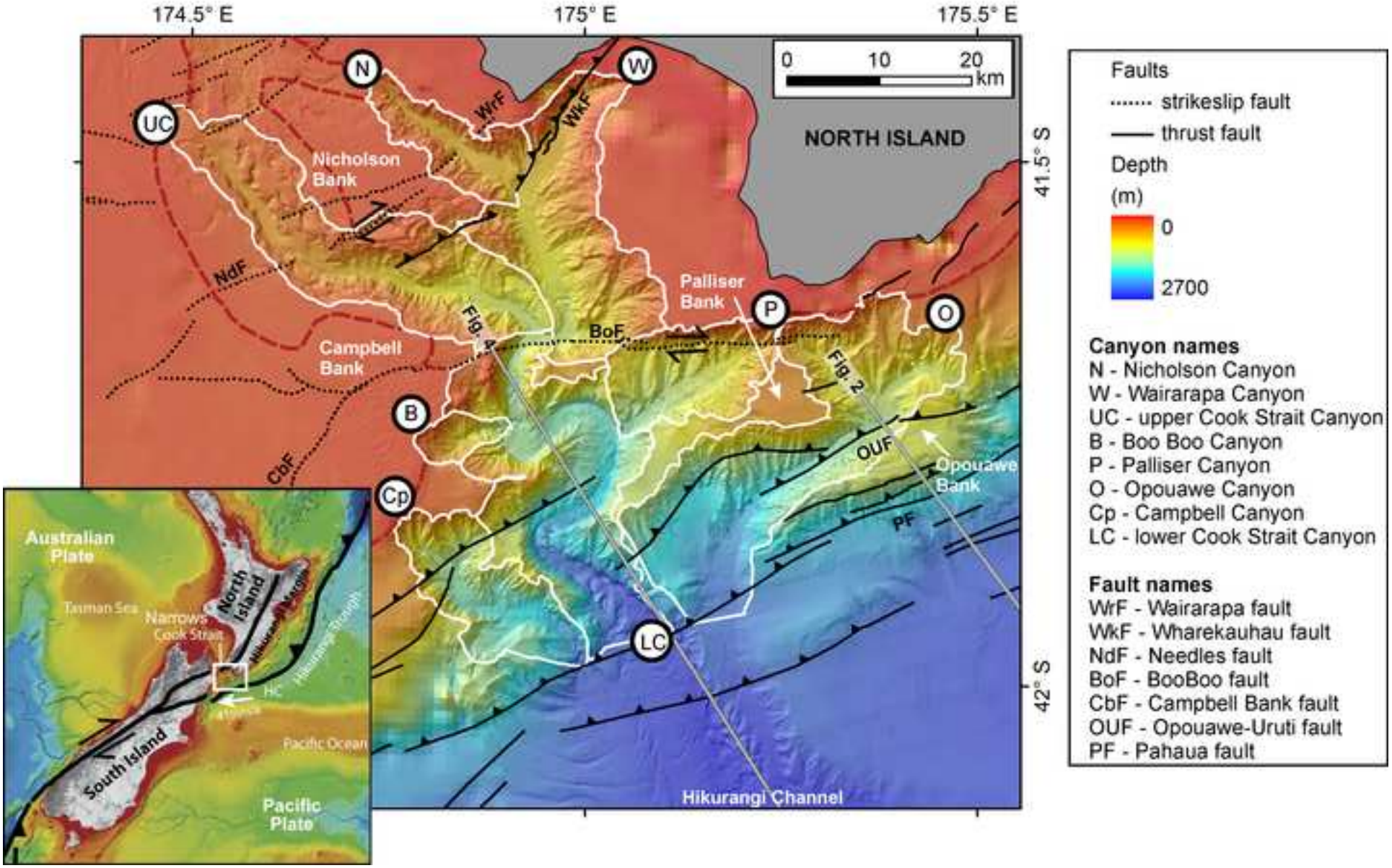

Figure 2
Click here to download high resolution image

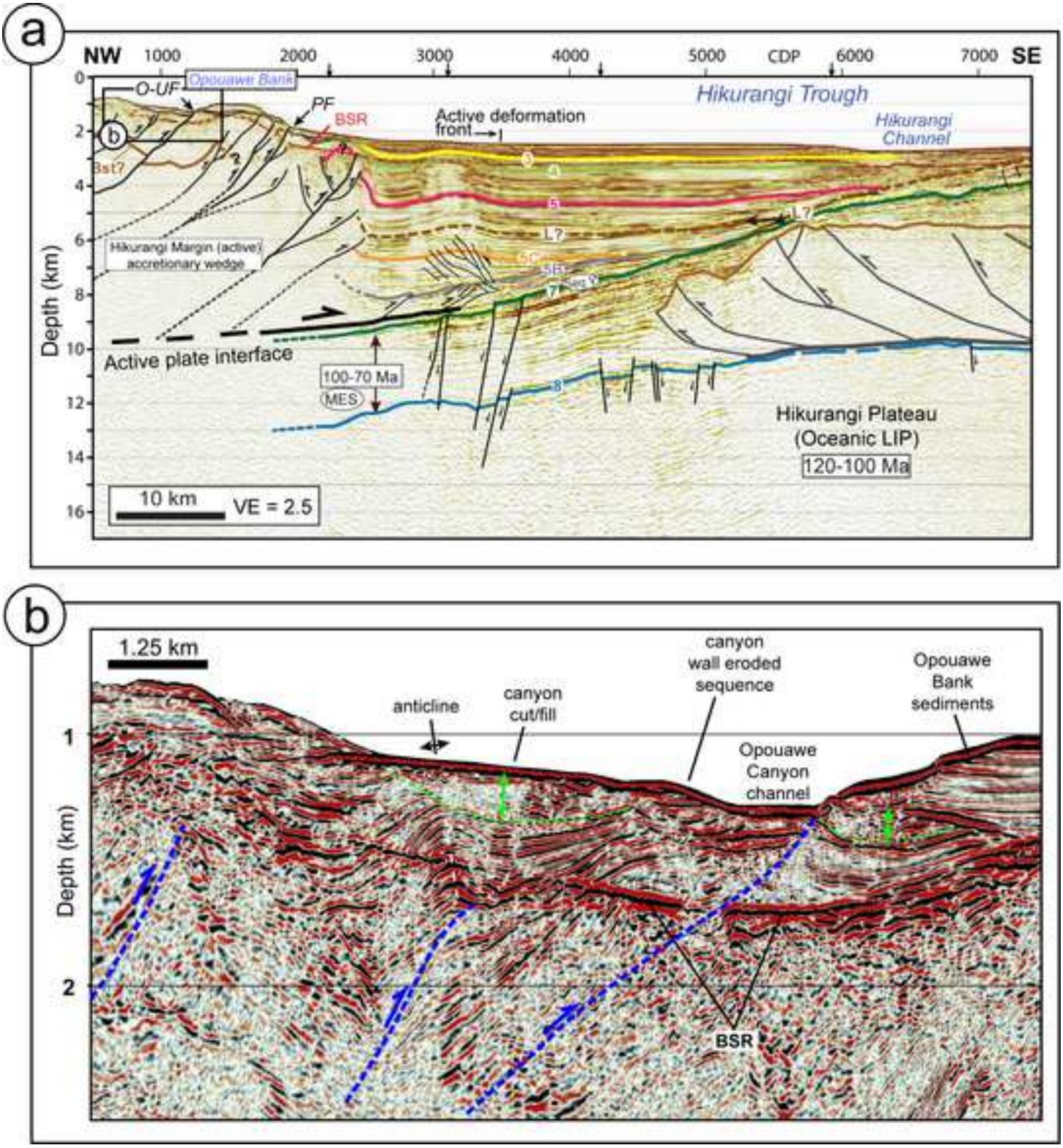

Figure 3
Click here to download high resolution image

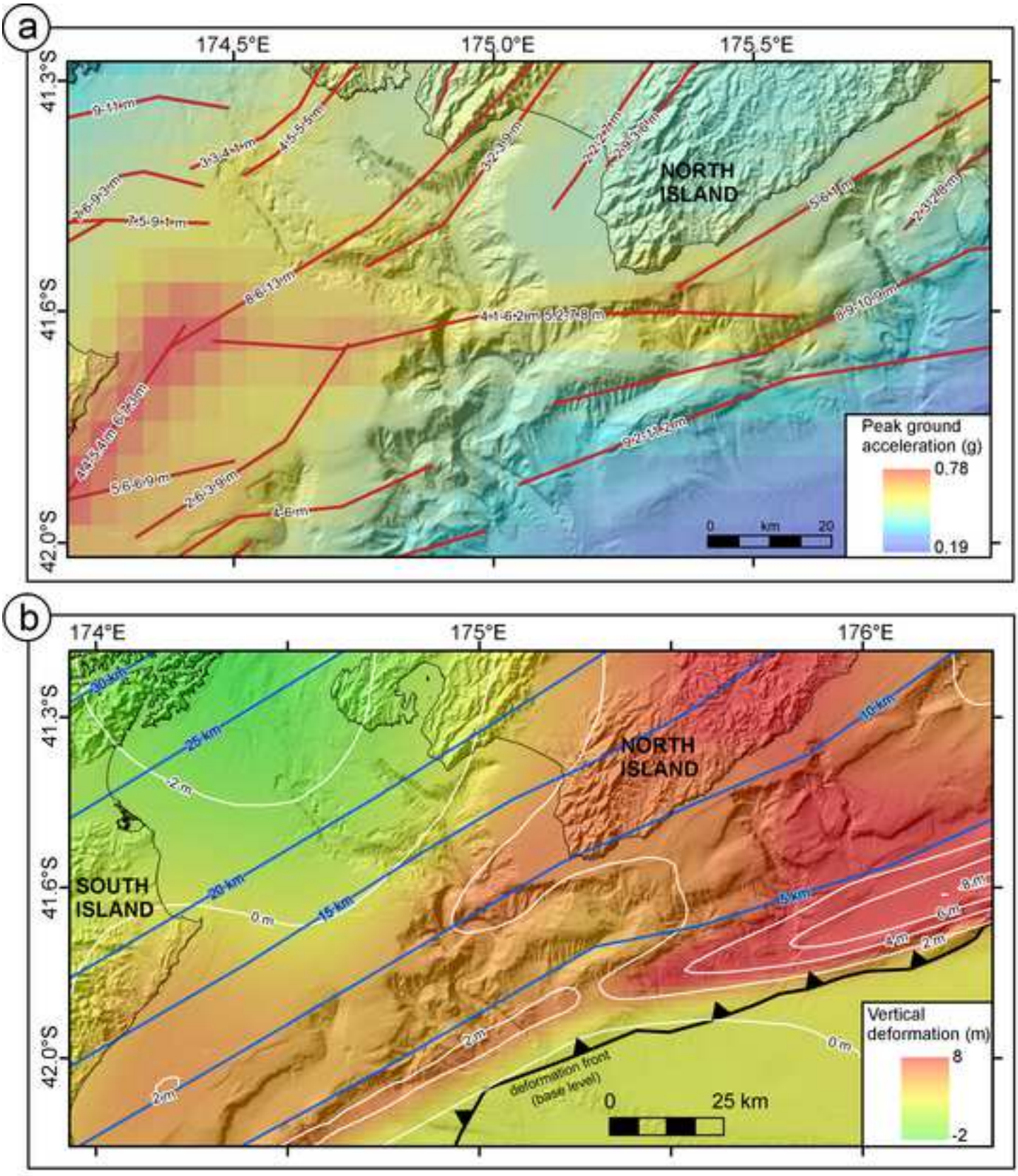

Figure 4

Click here to download high resolution image

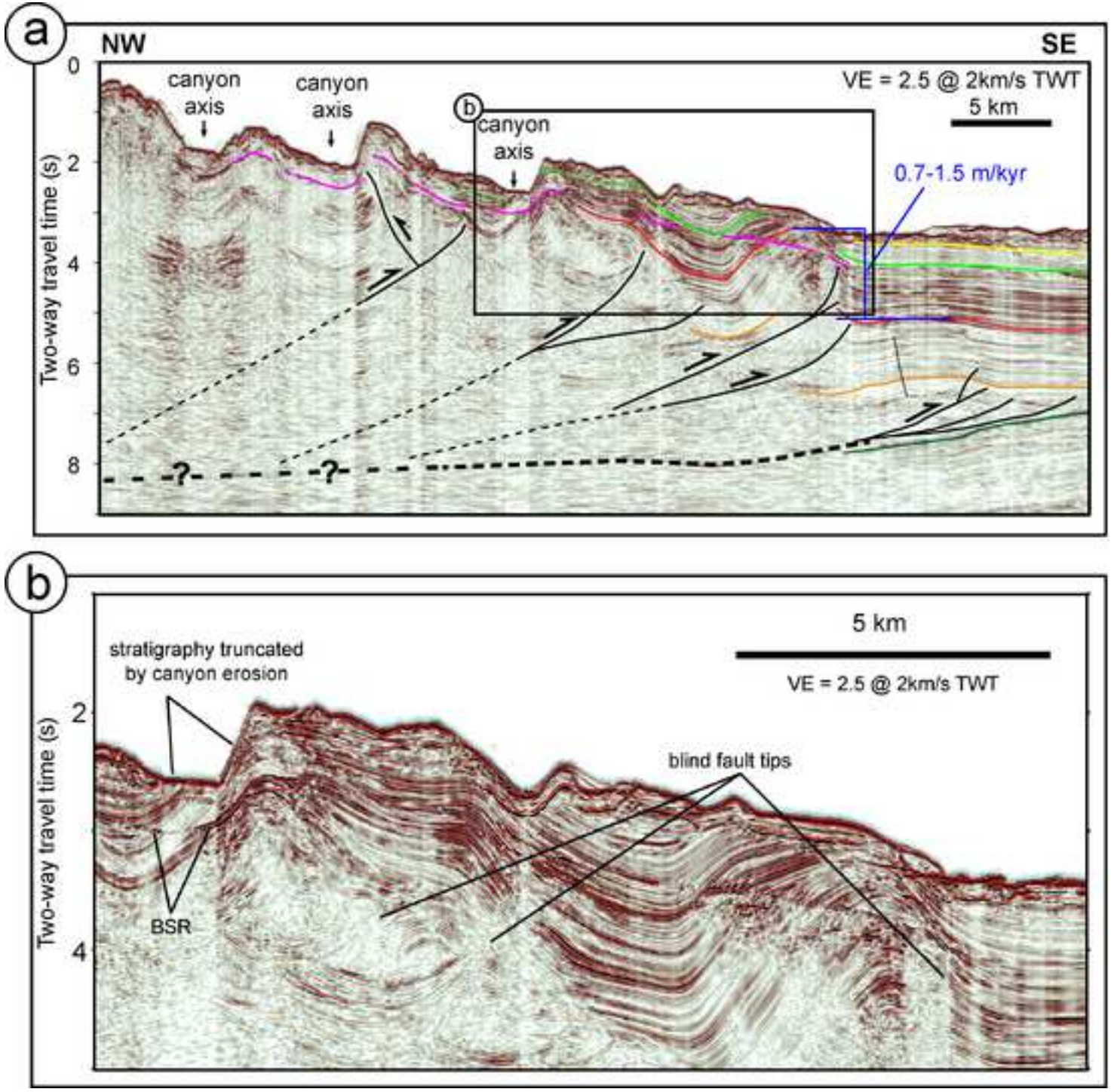

Figure 5-PartA

Click here to download high resolution image

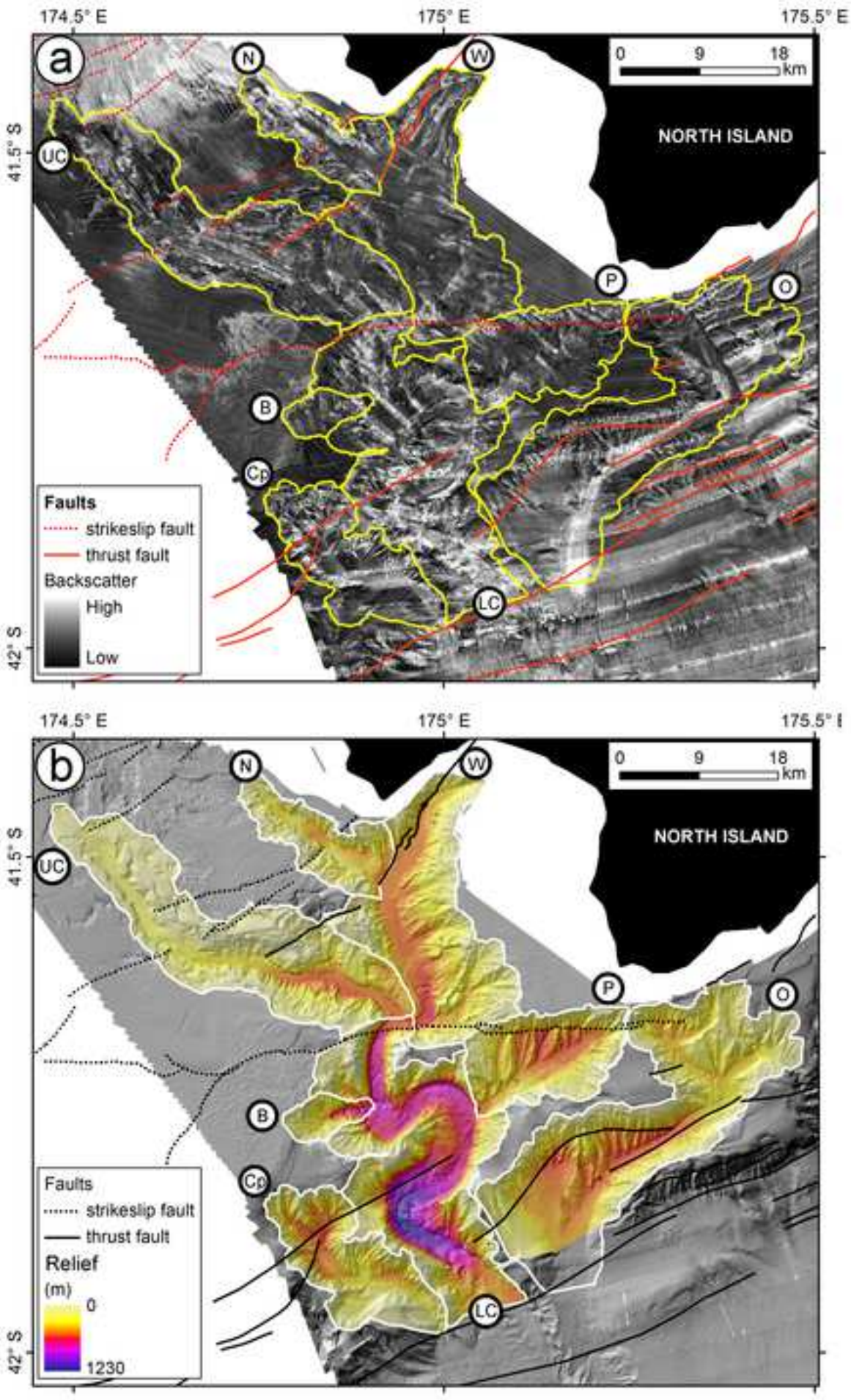

Figure 5-PartB

Click here to download high resolution image

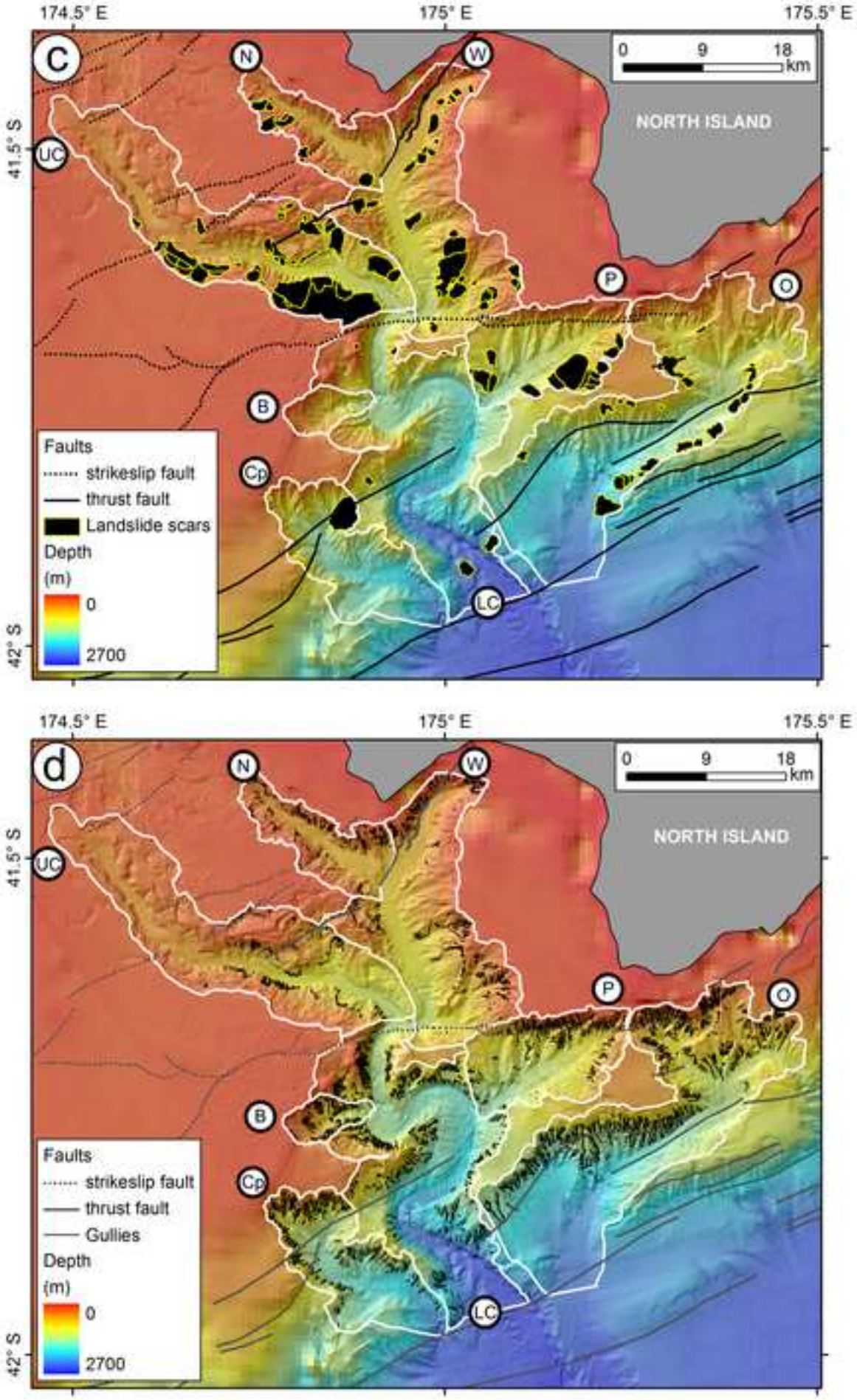

Figure 6
Click here to download high resolution image

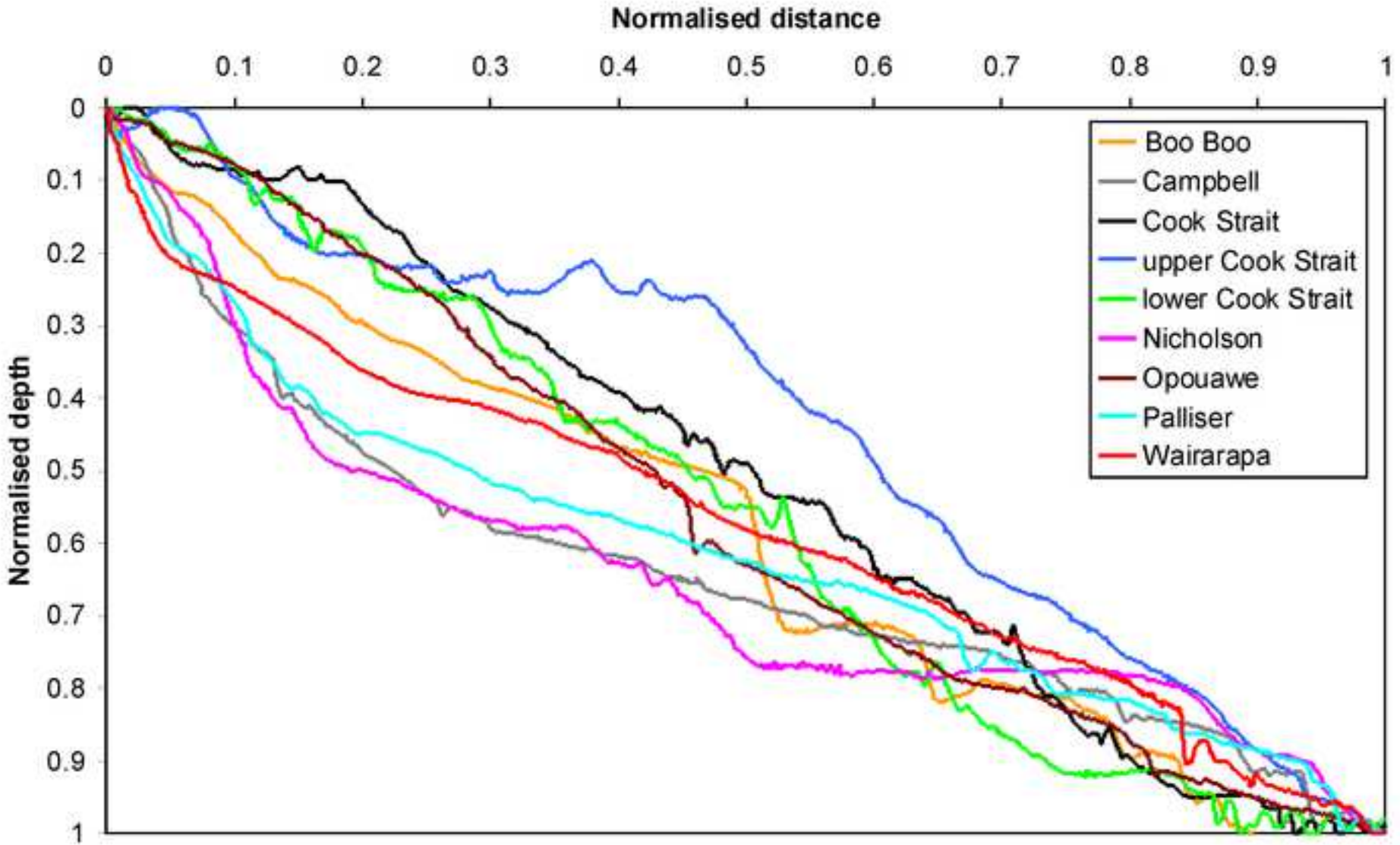

Figure 7-PartA
Click here to download high resolution image

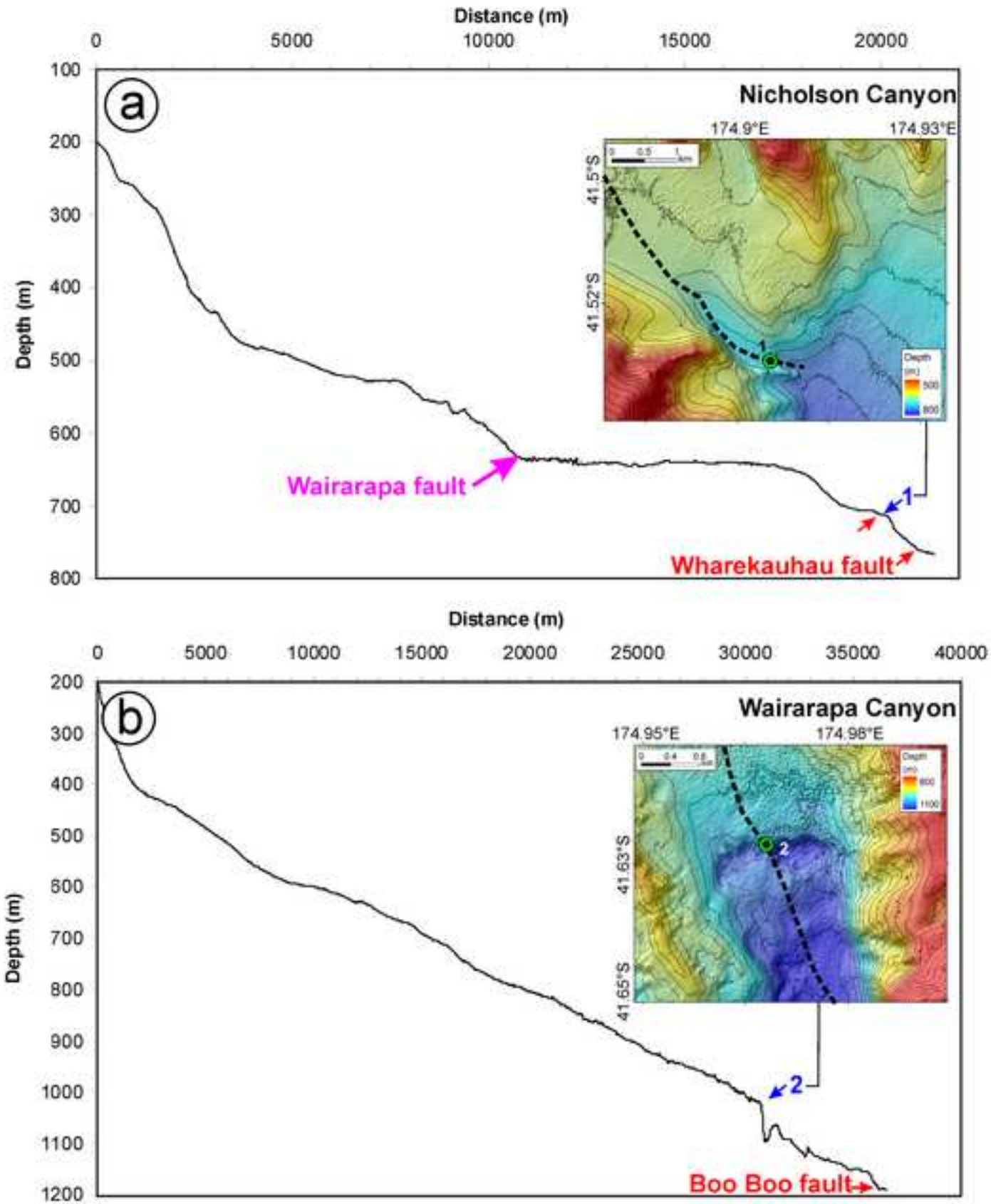

Figure 7-PartB
Click here to download high resolution image

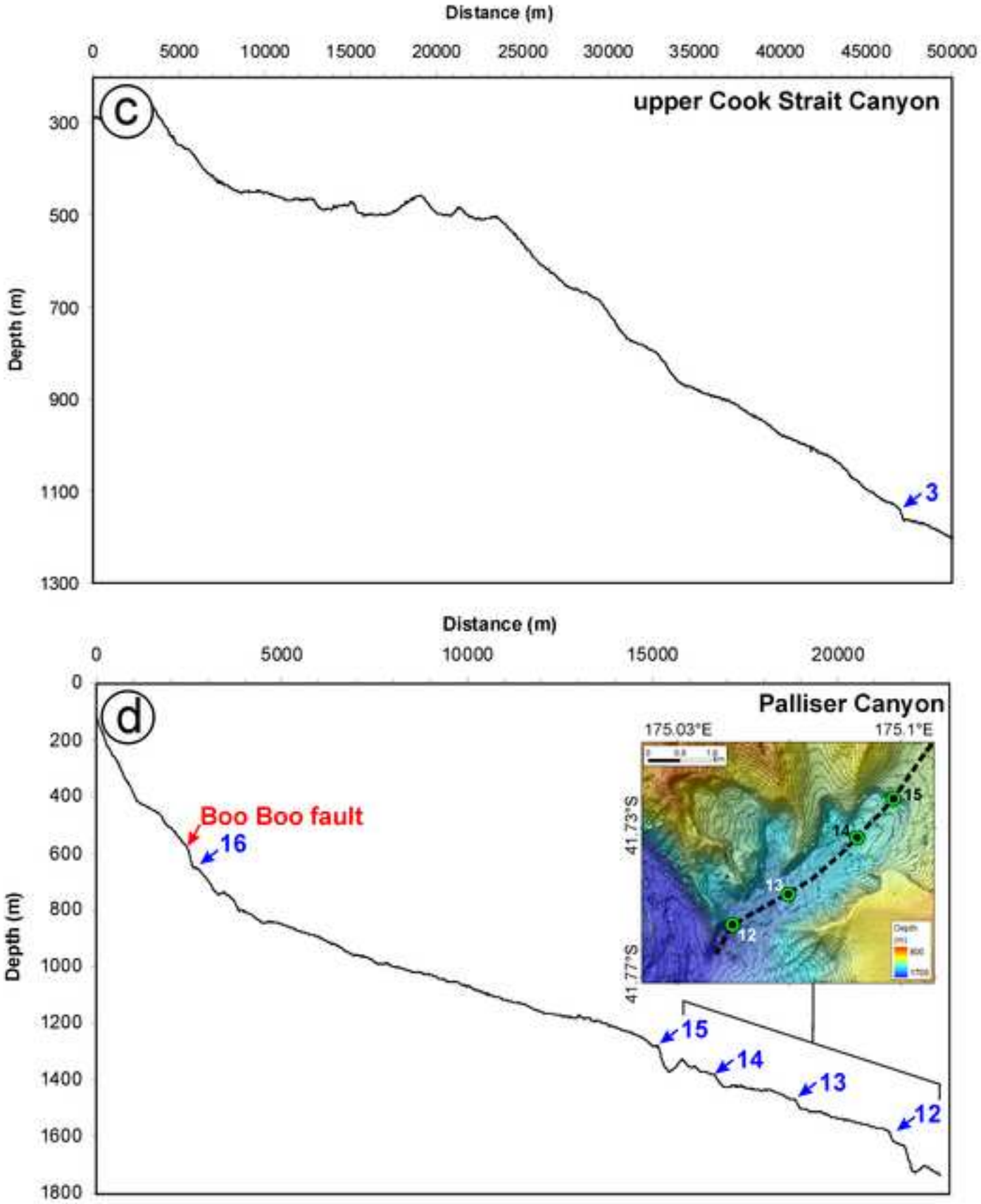

Figure 7-PartC
Click here to download high resolution image

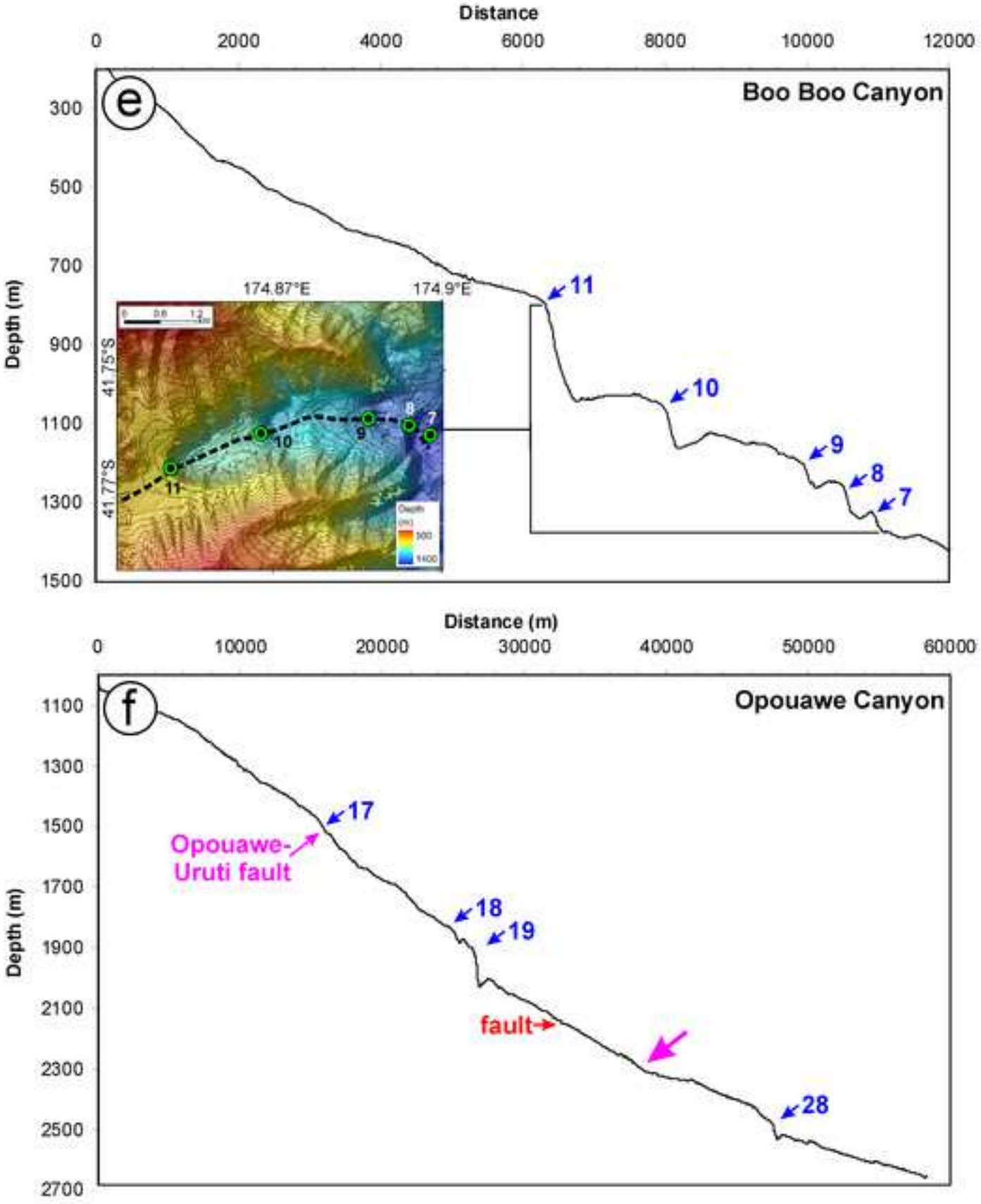

Figure 7-PartD
Click here to download high resolution image

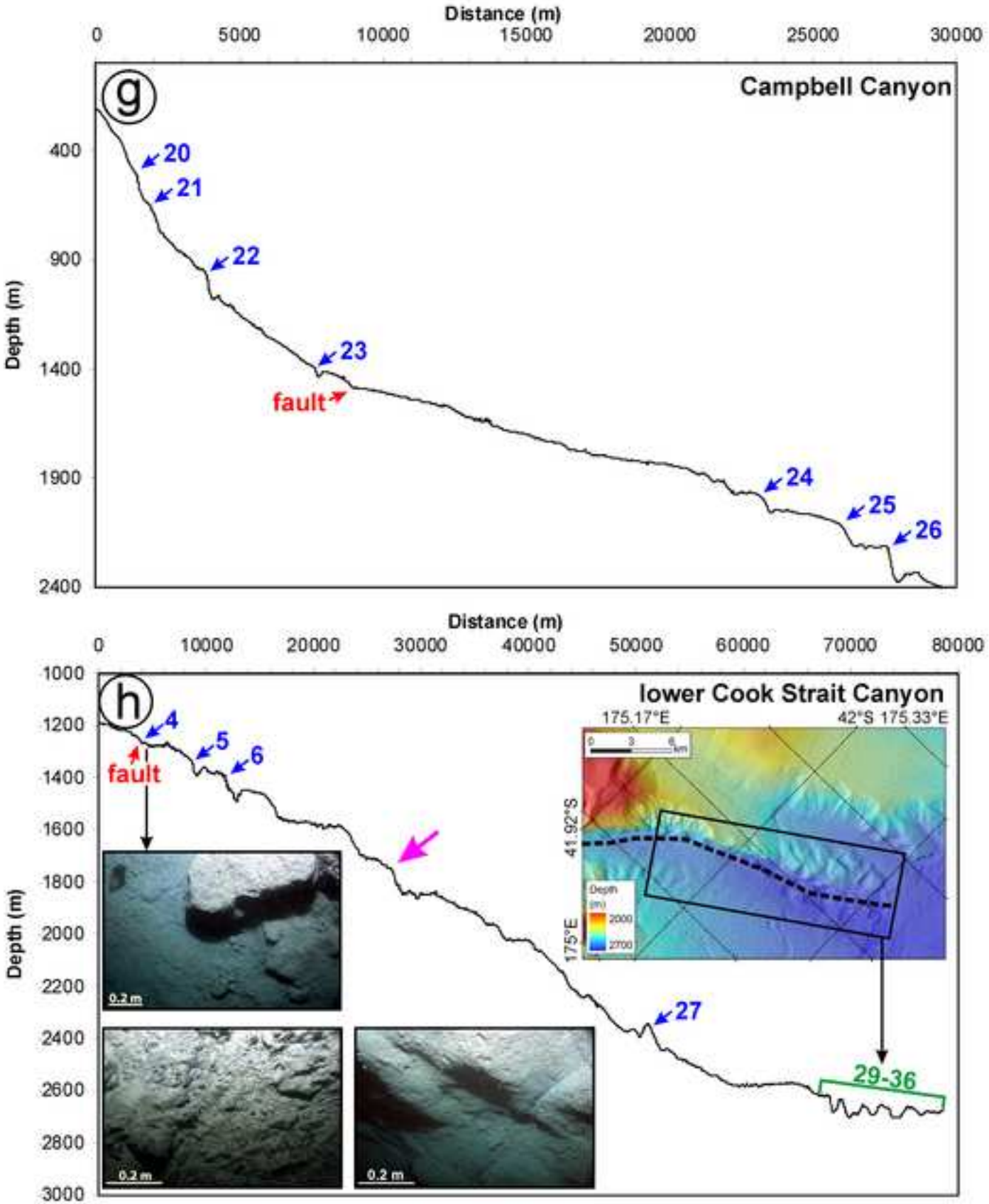

Figure 8

Click here to download high resolution image

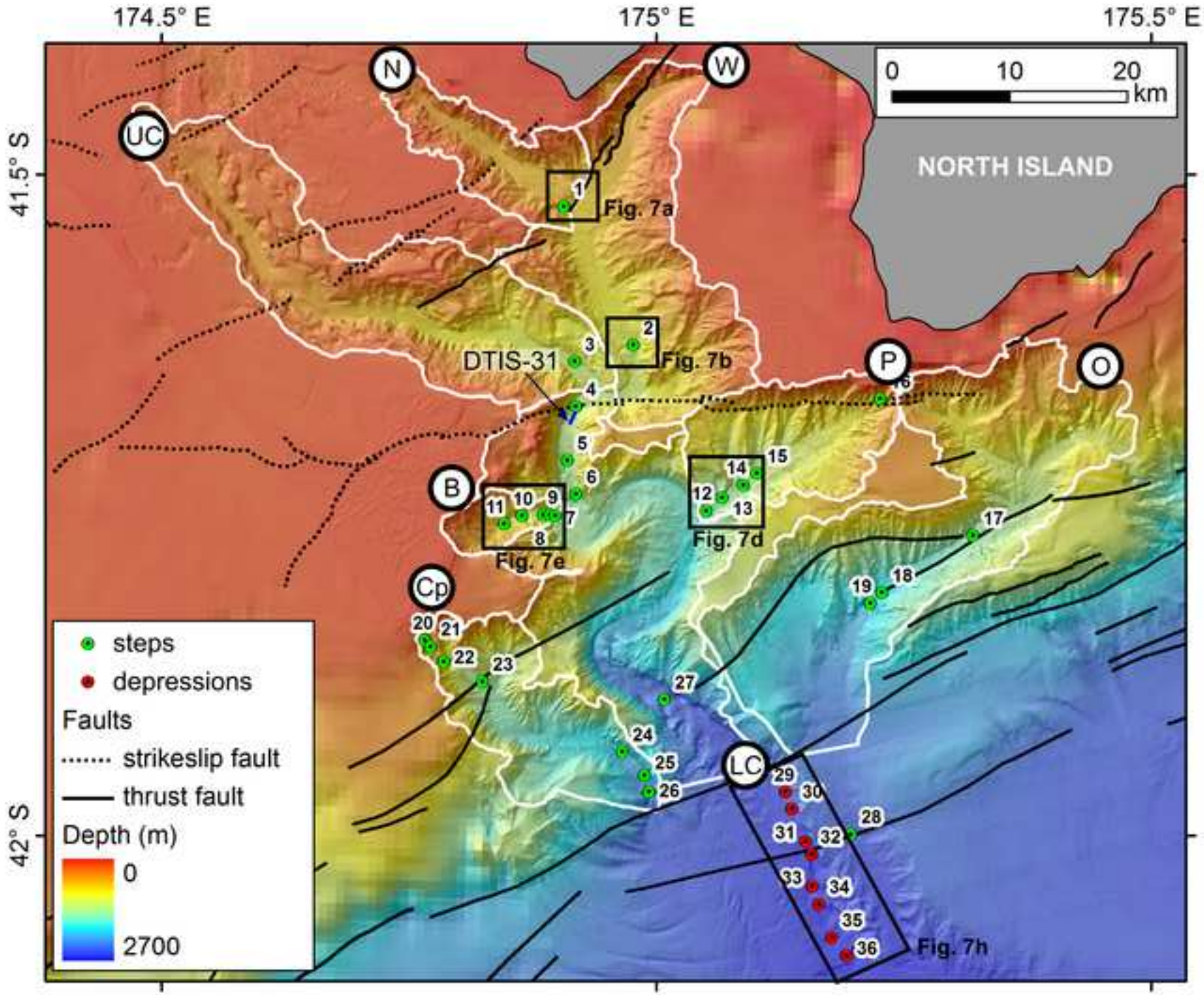

Figure 9
Click here to download high resolution image

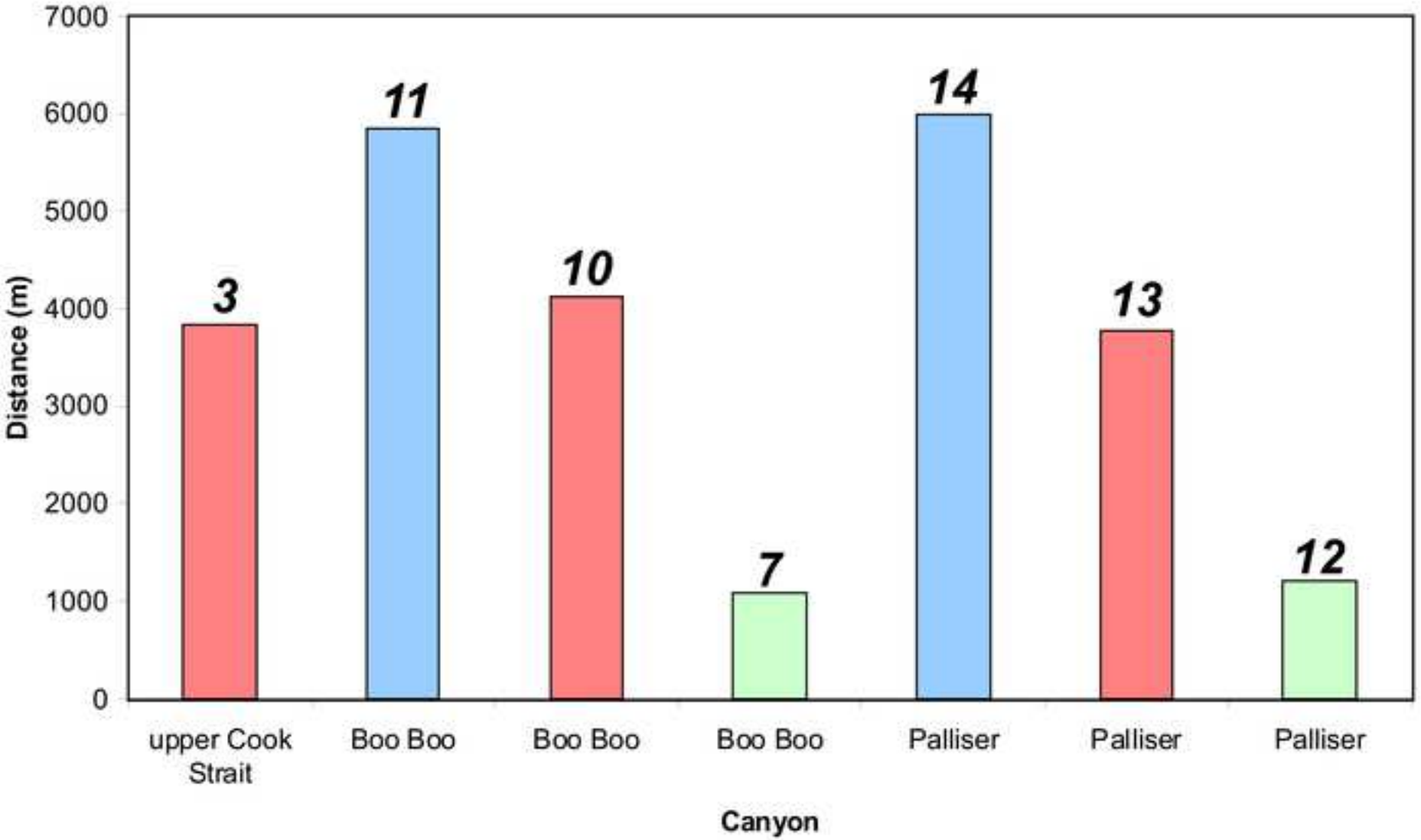

Figure 10
Click here to download high resolution image

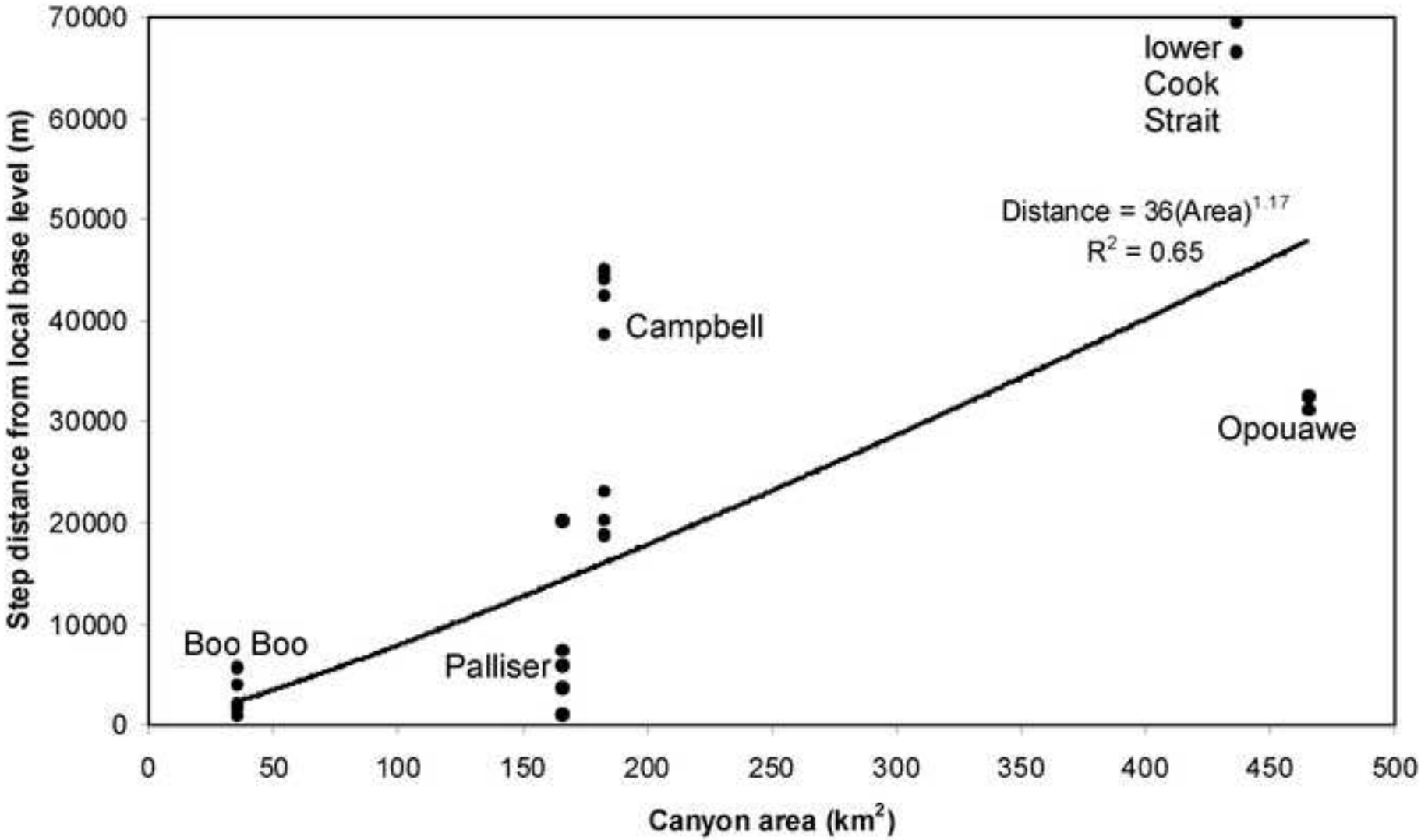

Figure 11-PartA

Click here to download high resolution image

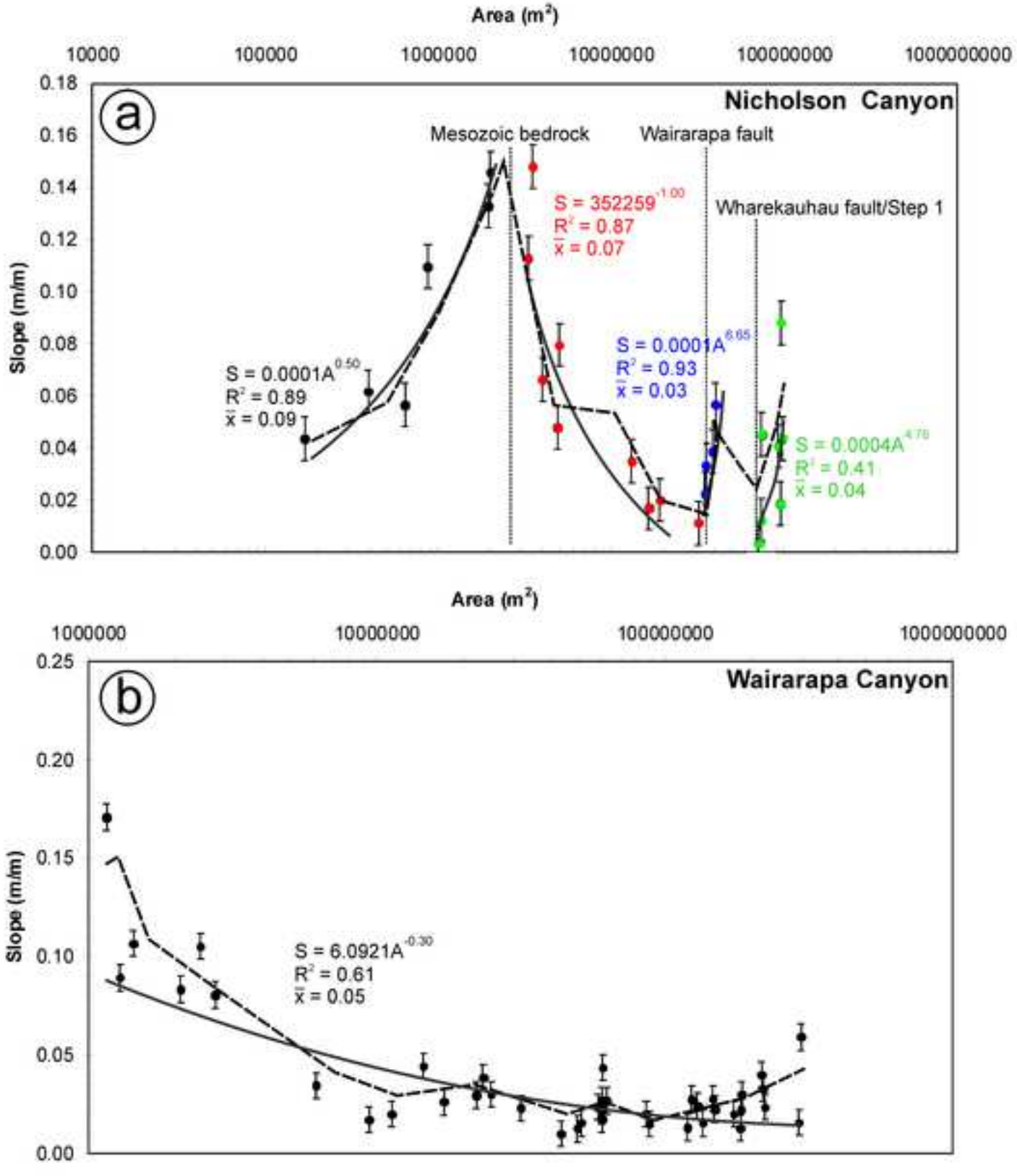

Figure 11-PartB
Click here to download high resolution image

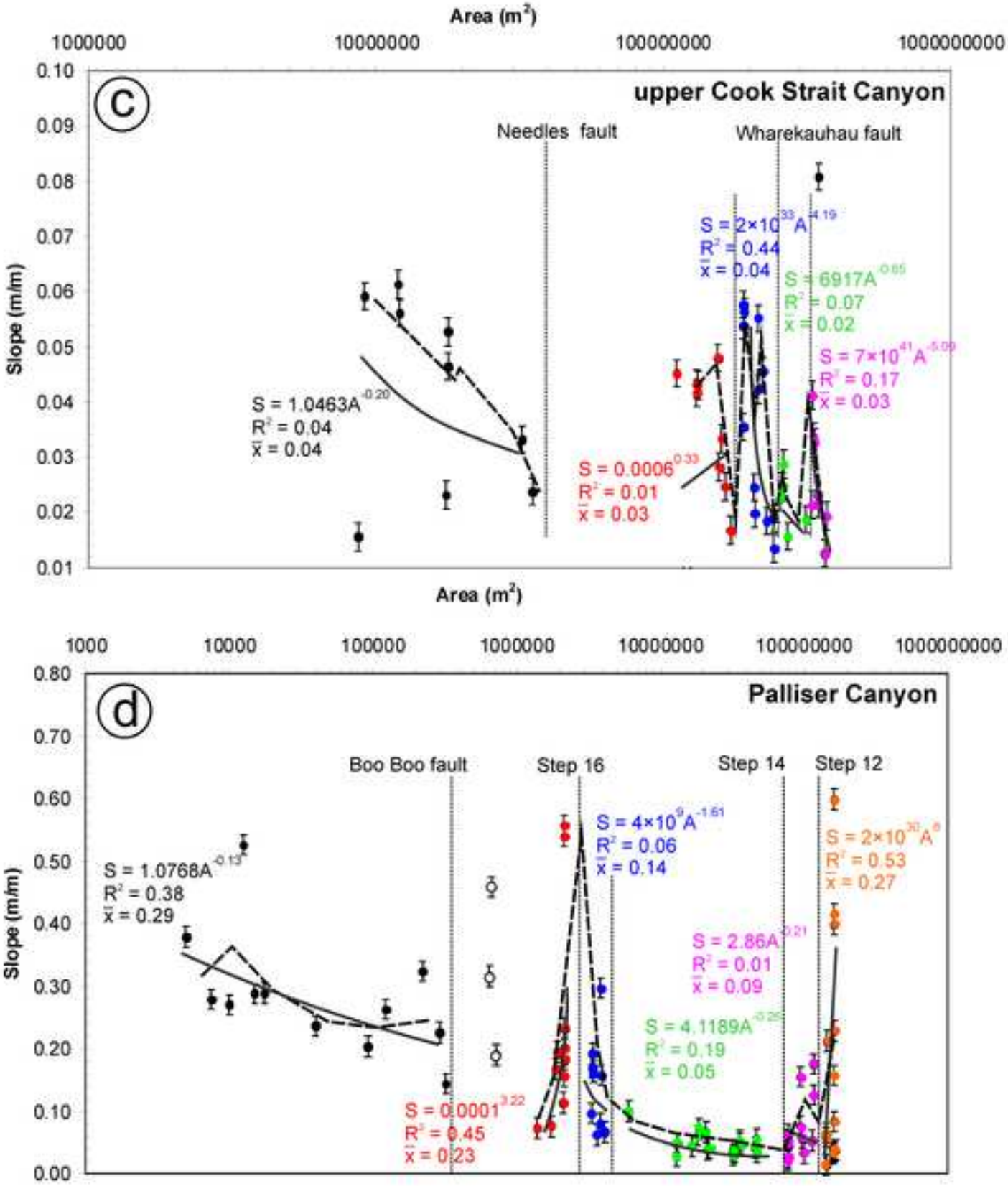

Figure 11-PartC
Click here to download high resolution image

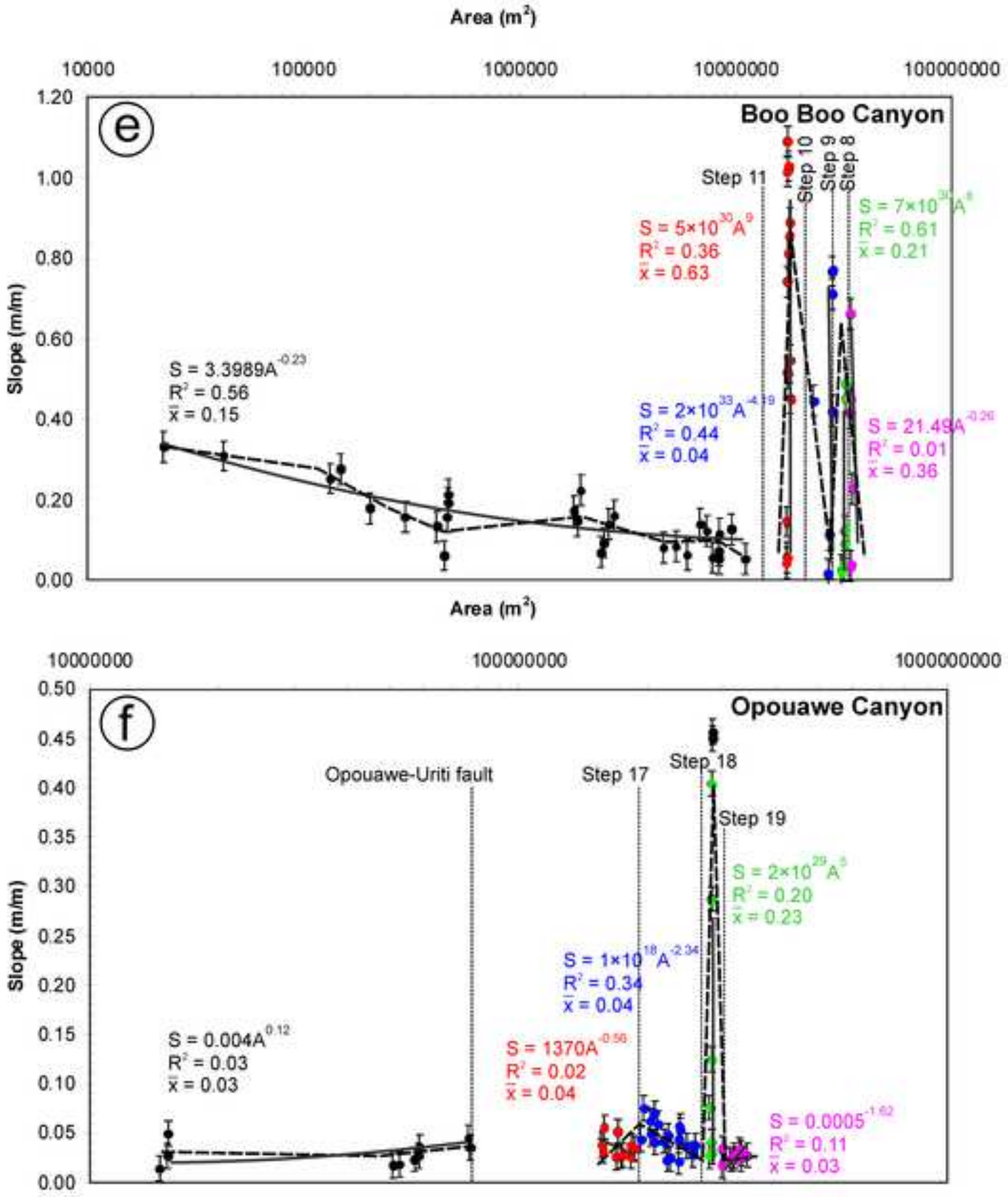

Figure 11-PartD
Click here to download high resolution image

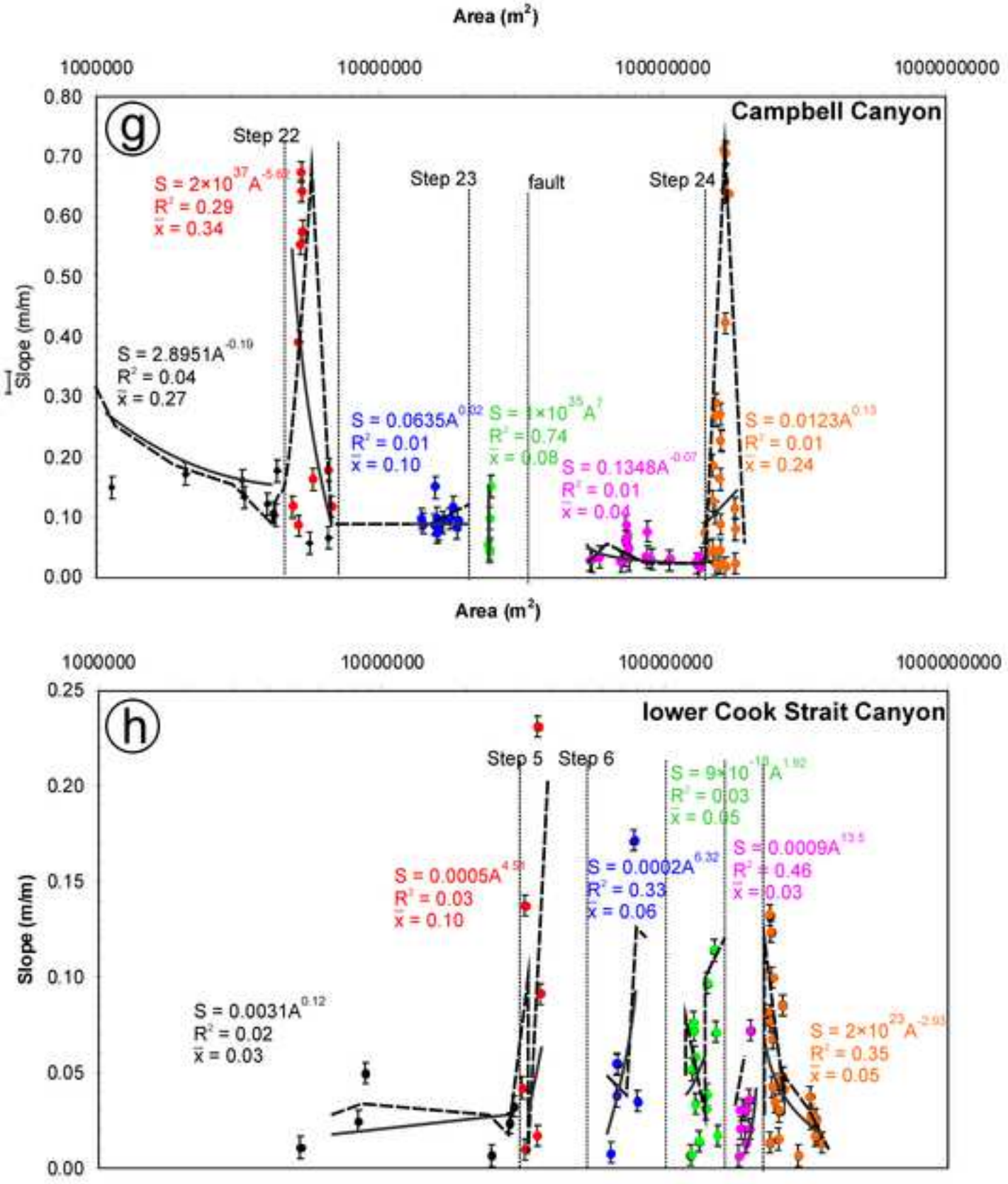

Figure 12

Click here to download high resolution image

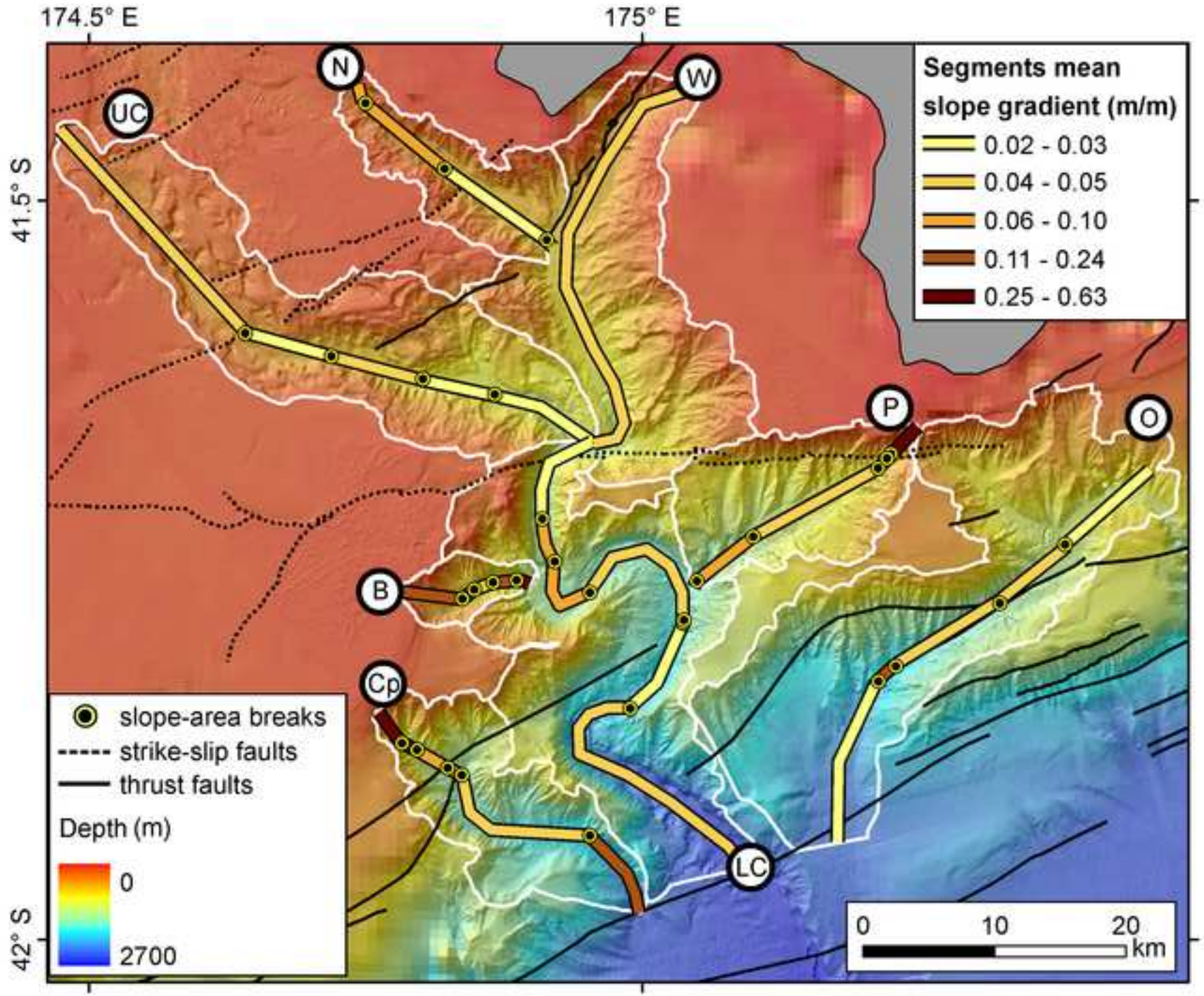

Figure 13
Click here to download high resolution image